



Genome-wide association analyses identify new Brugada syndrome risk loci and highlight a new mechanism of sodium channel regulation in disease susceptibility

Julien Barc, Rafik Tadros, Charlotte Glinge, David Chiang, Mariam Jouni, Floriane Simonet, Sean Jurgens, Manon Baudic, Michele Nicastro, Franck Potet, et al.

► To cite this version:

Julien Barc, Rafik Tadros, Charlotte Glinge, David Chiang, Mariam Jouni, et al.. Genome-wide association analyses identify new Brugada syndrome risk loci and highlight a new mechanism of sodium channel regulation in disease susceptibility. *Nature Genetics*, 2022, 54 (3), pp.232-239. <10.1038/s41588-021-01007-6>. <hal-03589076>

HAL Id: hal-03589076

<https://hal.science/hal-03589076v1>

Submitted on 29 Mar 2022

HAL is a multi-disciplinary open access archive for the deposit and dissemination of scientific research documents, whether they are published or not. The documents may come from teaching and research institutions in France or abroad, or from public or private research centers.

L'archive ouverte pluridisciplinaire **HAL**, est destinée au dépôt et à la diffusion de documents scientifiques de niveau recherche, publiés ou non, émanant des établissements d'enseignement et de recherche français ou étrangers, des laboratoires publics ou privés.



HAL Authorization

Barc J, Tadros R, Glinge C, Chiang DY, Jouni M, Simonet F, Jurgens SJ, Baudic M, Nicastro M, Potet F, Offerhaus JA, Walsh R, Choi SH, Verkerk AO, Mizusawa Y, Anys S, Minois D, Arnaud M, Duchateau J, Wijeyeratne YD, Muir A, Papadakis M, Castelletti S, Torchio M, Ortuño CG, Lacunza J, Giachino DF, Cerrato N, Martins RP, Campuzano O, Van Dooren S, Thollet A, Kyndt F, Mazzanti A, Clémenty N, Bisson A, Corveleyn A, Stallmeyer B, Dittmann S, Saenen J, Noël A, Honarbakhsh S, Rudic B, Marzak H, Rowe MK, Federspiel C, Le Page S, Placide L, Milhem A, Barajas-Martinez H, Beckmann BM, Krapels IP, Steinfurt J, Winkel BG, Jabbari R, Shoemaker MB, Boukens BJ, Škorić-Milosavljević D, Bikker H, Manevy FC, Lichtner P, Ribasés M, Meitinger T, Müller-Nurasyid M; KORA-Study Group, Veldink JH, van den Berg LH, Van Damme P, Cusi D, Lanzani C, Rigade S, Charpentier E, Baron E, Bonnaud S, Lecointe S, Donnart A, Le Marec H, Chatel S, Karakachoff M, Bézieau S, London B, Tfelt-Hansen J, Roden D, Odening KE, Cerrone M, Chinitz LA, Volders PG, van de Berg MP, Laurent G, Faivre L, Antzelevitch C, Kääh S, Arnaout AA, Dupuis JM, Pasquie JL, Billon O, Roberts JD, Jesel L, Borggrefe M, Lambiase PD, Mansourati J, Loeys B, Leenhardt A, Guicheney P, Maury P, Schulze-Bahr E, Robyns T, Breckpot J, Babuty D, Priori SG, Napolitano C; Nantes Referral Center for inherited cardiac arrhythmia, de Asmundis C, Brugada P, Brugada R, Arbelo E, Brugada J, Mabo P, Behar N, Giustetto C, Molina MS, Gimeno JR, Hasdemir C, Schwartz PJ, Crotti L, McKeown PP, Sharma S, Behr ER, Haissaguerre M, Sacher F, Rooryck C, Tan HL, Remme CA, Postema PG, Delmar M, Ellinor PT, Lubitz SA, Gourraud JB, Tanck MW, George AL Jr, MacRae CA, Burridge PW, Dina C, Probst V, Wilde AA, Schott JJ, Redon R, Bezzina CR.

Genome-wide association analyses identify new Brugada syndrome risk loci and highlight a new mechanism of sodium channel regulation in disease susceptibility

Genome-wide association analyses identify new Brugada syndrome risk loci and highlight a new mechanism of sodium channel regulation in disease susceptibility

Brugada syndrome (BrS) is a cardiac arrhythmia disorder associated with sudden death in young adults. With the exception of *SCN5A*, encoding the cardiac sodium channel $\text{Na}_v1.5$, susceptibility genes remain largely unknown. Here we performed a genome-wide association meta-analysis comprising 2,820 unrelated cases with BrS and 10,001 controls, and identified 21 association signals at 12 loci (10 new). Single nucleotide polymorphism (SNP)-heritability estimates indicate a strong polygenic influence. Polygenic risk score analyses based on the 21 susceptibility variants demonstrate varying cumulative contribution of common risk alleles among different patient subgroups, as well as genetic associations with cardiac electrical traits and disorders in the general population. The predominance of cardiac transcription factor loci indicates that transcriptional regulation is a key feature of BrS pathogenesis. Furthermore, functional studies conducted on *MAPRE2*, encoding the microtubule plus-end binding protein EB2, point to microtubule-related trafficking effects on $\text{Na}_v1.5$ expression as a new underlying molecular mechanism. Taken together, these findings broaden our understanding of the genetic architecture of BrS and provide new insights into its molecular underpinnings.

BrS is a cardiac disorder characterized by hallmark ST-segment elevation in the right precordial leads of the electrocardiogram (ECG) and increased risk of sudden death in young adults^{1,2}. Rare coding variants in *SCN5A*, encoding the cardiac sodium channel $\text{Na}_v1.5$ that underlies the sodium current (I_{Na}), are reported in approximately 20% of cases^{3,4}. Other susceptibility genes contributing to the disorder remain largely unknown. In a genome-wide association study (GWAS) conducted in 312 individuals with BrS, we previously identified three common susceptibility variants and provided evidence for a complex genetic architecture⁵. Here, we extended this original association scan to a large meta-analysis comprising 2,820 unrelated cases and 10,001 controls of European ancestry (Supplementary Tables 1 and 2 and Supplementary Note), testing 6,990,521 variants with a minor allele frequency (MAF) ≥ 0.01 (Fig. 1 and Supplementary Figs. 1 and 2). A total of 12 loci (10 new) reached the genome-wide statistical significance threshold of $P < 5 \times 10^{-8}$ (Table 1 and Supplementary Fig. 3a–l). Conditional analysis uncovered seven additional association signals at genome-wide significance at the chromosome 3 locus, and an additional signal at the chromosome 6 and chromosome 7 loci (Table 1 and Supplementary Fig. 3m–u). Analysis of SNP-based heritability (h^2_{SNP}) demonstrated that a substantial portion of susceptibility to BrS is attributable to common genetic variation. h^2_{SNP} estimates ranged from

0.17 (s.e. 0.035) using LDSC⁶ to 0.34 (s.e. 0.02) using GREML⁷, assuming a disease prevalence of 0.05%⁸, with 24% of the total SNP-based heritability being explained by the 12 loci reaching genome-wide significance (Supplementary Table 4).

Seven association signals (defined by the lead SNP and SNPs with $r^2 \geq 0.6$) at the chromosome 3 locus overlapped *SCN5A* and one overlapped the neighboring *SCN10A* gene encoding the sodium channel isoform $\text{Na}_v1.8$ (Supplementary Fig. 4a–h). Although previous work⁹ proposed that the latter signal may act through regulation of *SCN5A* expression, a possible involvement of *SCN10A* itself is suggested by a significant expression quantitative trait loci (eQTL) in left ventricular tissue ($P = 5.29 \times 10^{-6}$, colocalization posterior probability (CLPP) = 0.16) (Supplementary Fig. 4h and Supplementary Table 3), whereas no eQTL was detected for *SCN5A* ($P = 0.27$). Notably, six association signals overlapped genes encoding cardiac developmental transcription factors (*HEY2*, *TBX20*, *ZFPM2*, *GATA4*, *WT1*, *TBX5*) and four were < 300 kb from such genes (*TBX20*, *IRX3/IRX5*, *HEY2*)¹⁰. In support of the involvement of transcription factor genes, an enrichment in genes encoding DNA-binding proteins was found at BrS GWAS loci by permutation testing (one-tailed permutation $P = 1 \times 10^{-4}$; Extended Data Fig. 1). The transcription factors *HEY2*, *TBX20*, *GATA4*, *TBX5* and *IRX3/IRX5* are established regulators of ion-channel expression in the adult heart, including that of $\text{Na}_v1.5$ (refs. 11–15), suggesting that modulation of ion-channel expression is an important mechanism in BrS. Potential regulatory effects of the transcription factors *WT1* and *ZFPM2* on ion-channel expression have not yet been investigated. One association signal overlapped *PRKCA* (supported by a colocating eQTL; $P = 4.63 \times 10^{-28}$, CLPP = 0.99) (Supplementary Fig. 4s and Supplementary Table 3), which encodes protein kinase C alpha involved in contractility and calcium handling in cardiomyocytes¹⁶. Lastly, two association signals overlapped genes encoding microtubule- or myofiber-associated proteins, namely *MAPRE2* (ref. 17) and *MYO18B* (ref. 18). A full annotation of the association signals (Methods) is presented in Supplementary Table 3 and Supplementary Fig. 4.

We performed a transcriptome-wide analysis (TWAS)¹⁹ based on predicted gene expression in cardiac tissues²⁰ and identified 24 associations corresponding to 20 unique genes at the Bonferroni-corrected threshold of $P < 5.2 \times 10^{-6}$ (Supplementary Table 5). Eighteen of these genes are within ~ 0.5 Mb of GWAS signals while two point to additional loci (Supplementary Table 5). MAGMA gene property analysis for tissue specificity²¹ as well as enrichment analysis using LDSC-SEQ²² and GARFIELD²³ identified left ventricle, right ventricle and fetal heart, respectively, as significantly associated with BrS (Supplementary Figs. 5 and 6 and

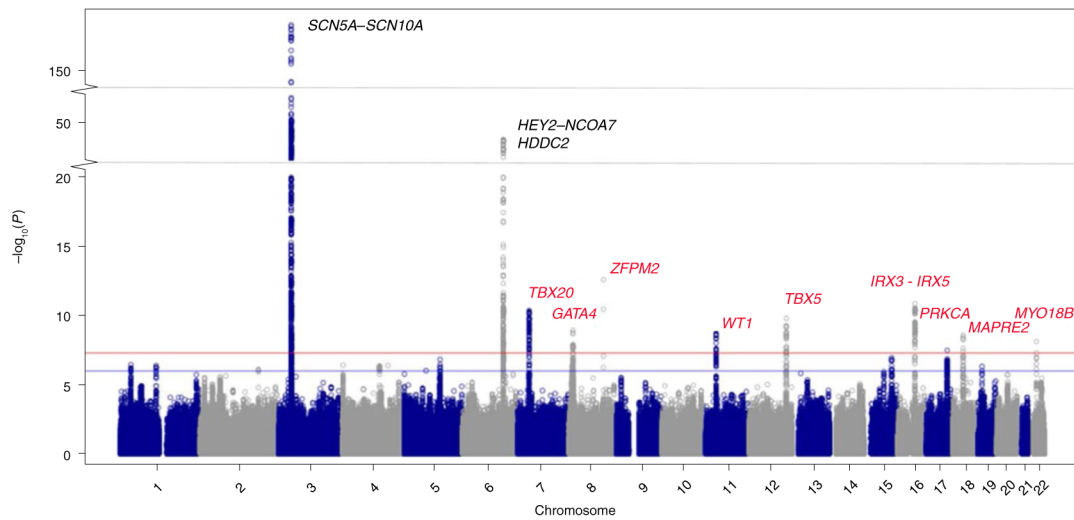


Fig. 1 | Manhattan plot of genome-wide association meta-analysis comprising 2,820 unrelated BrS cases and 10,001 controls. The association P values were derived from a meta-analysis of the ten GWAS strata using a fixed-effects model with an inverse-variance weighted approach. We performed logistic regression on the disease status under an additive model of SNP's genotype. P values are two-sided and not adjusted for multiple testing. The y axis has breaks to emphasize the new loci. The red and blue lines indicate the genome-wide significance ($P < 5 \times 10^{-8}$) and suggestive significance ($P < 1 \times 10^{-6}$) thresholds, respectively. Genes at new loci are depicted in red.

Table 1 | Lead SNPs and effect estimates for genome-wide significant association signals ($P < 5 \times 10^{-8}$) in the BrS GWAS meta-analysis

Locus	Lead SNP	Genomic position (hg19)	Risk allele	Other allele	Risk allele frequency in cases	Risk allele frequency in controls	OR (95% CI) ^b	P value	Nearest gene
1	rs7638909 ^a	3:38594973	G	T	0.32	0.24	1.28 (1.17-1.40)	2.79×10^{-8}	SCN5A
	rs62241190 ^a	3:38607468	G	A	0.06	0.03	1.96 (1.63-2.32)	8.56×10^{-14}	SCN5A
	rs7374540 ^a	3:38634142	C	A	0.51	0.39	1.72 (1.61-1.81)	3.56×10^{-57}	SCN5A
	rs7433206 ^a	3:38657708	A	T	0.45	0.42	1.48 (1.37-1.60)	9.52×10^{-24}	SCN5A
	rs34760424 ^a	3:38683018	G	T	0.98	0.94	2.32 (1.96-2.70)	3.03×10^{-23}	SCN5A
	rs41310232 ^a	3:38689242	A	G	0.16	0.09	1.56 (1.40-1.74)	1.19×10^{-15}	SCN5A
	rs6782237 ^a	3:38696553	C	G	0.78	0.68	1.74 (1.61-1.87)	1.05×10^{-47}	SCN5A
	rs6801957	3:38767315	T	C	0.65	0.42	2.49 (2.34-2.65)	1.30×10^{-180}	SCN10A
2	rs6913204 ^a	6:125664540	C	T	0.51	0.47	1.22 (1.13-1.29)	1.30×10^{-8}	HSDC2
	rs9398791	6:126115821	C	T	0.61	0.51	1.53 (1.44-1.63)	1.49×10^{-39}	HEY2, NCOA7
3	rs11765936	7:35349146	G	T	0.18	0.15	1.37 (1.25-1.49)	4.30×10^{-11}	TBX20
	rs340398 ^a	7:35413788	C	T	0.42	0.38	1.22 (1.15-1.30)	1.76×10^{-9}	TBX20
4	rs804281	8:11611865	G	A	0.63	0.58	1.22 (1.15-1.30)	1.22×10^{-9}	GATA4
5	rs72671655	8:106347897	T	A	0.97	0.95	1.85 (1.59-2.22)	2.51×10^{-13}	ZFPM2
6	rs72905083	11:32474374	A	G	0.1	0.08	1.43 (1.27-1.60)	2.09×10^{-9}	WT1
7	rs883079	12:114793240	C	T	0.34	0.28	1.25 (1.16-1.33)	1.59×10^{-10}	TBX5
8	rs11645463	16:54456353	A	G	0.59	0.54	1.22 (1.15-1.30)	1.27×10^{-9}	IRX3
9	rs72622262	16:54662944	C	G	0.87	0.83	1.36 (1.25-1.49)	1.37×10^{-11}	CRNDE, IRX5
10	rs12945884	17:64300281	T	C	0.58	0.53	1.20 (1.12-1.28)	3.31×10^{-8}	PRKCA
11	rs476348	18:32670021	C	T	0.73	0.69	1.25 (1.16-1.33)	2.64×10^{-9}	MAPRE2
12	rs133902	22:26164079	T	C	0.48	0.43	1.21 (1.13-1.29)	7.73×10^{-9}	MYO18B

^a Variants associated with BrS in conditional analyses. ^b OR values refer to each unit increase in the risk allele. We performed logistic regression on the disease status under additive model of SNP's genotype. P values are two-sided and not adjusted for multiple testing. Confidence intervals are given for a nominal P value of 0.05 to allow comparability with other studies and reports.

Supplementary Tables 6 and 7). MAGMA gene-set analysis²¹ identified, among others, gene sets related to heart development and regulation of heart growth (Supplementary Table 8), which may point to a broader role of transcriptional dysregulation in the pathogenesis of BrS, beyond regulation of ion-channel expression.

MAPRE2 overlaps the association signal tagged by rs476348 and its causal role is supported by chromatin interaction between its promoter region and the association signal and by a significant eQTL ($P = 2.9 \times 10^{-5}$, CLPP = 0.10) (Extended Data Fig. 2 and Supplementary Table 3), where the BrS risk allele is associated

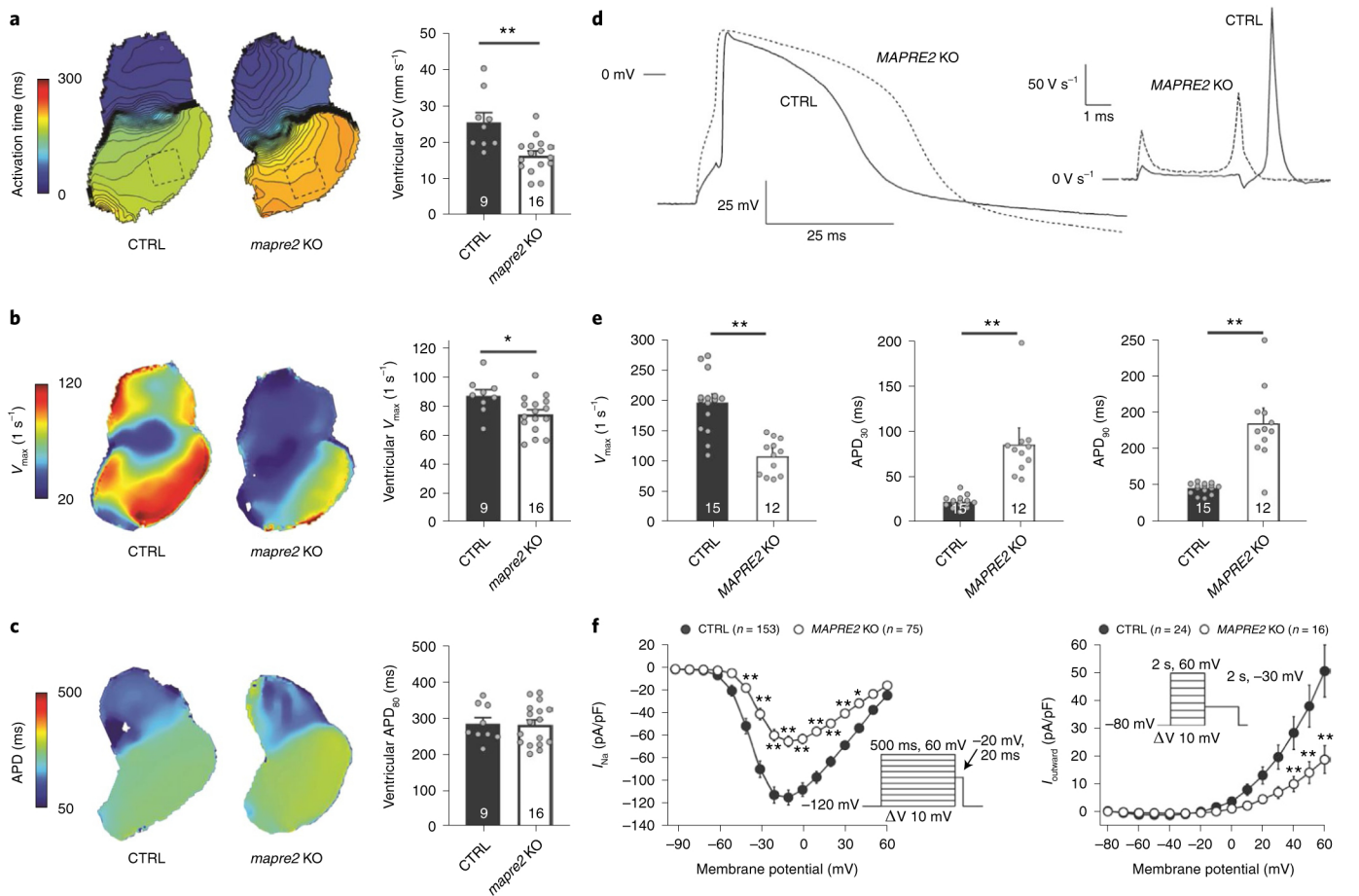


Fig. 2 | Loss of *MAPRE2* leads to lower CV, V_{max} and I_{Na} . **a**, (Left) Representative isochrone maps of hearts isolated from 5-day postfertilization zebrafish larvae injected with tracrRNA-Cas9 and multiple gRNAs targeting *mapre2* (*mapre2* KO) or tracrRNA-Cas9 without gRNA (CTRL). The dotted squares reflect the main ventricular area in the hearts from which the various parameters are measured. (Right) Average ventricular CV in CTRL and *mapre2* KO hearts. **b**, (Left) Representative maximum V_{max} maps from zebrafish hearts. (Right) Average V_{max} in CTRL and *mapre2* KO hearts. **c**, (Left) Representative maps of APD at 80% repolarization (APD₈₀) in isolated hearts paced at 100 b.p.m. (Right) Average APD₈₀ in CTRL and *mapre2* KO hearts. **d**, Representative APs at 1-Hz pacing from single hiPSC-CMs with CRISPR-Cas9-mediated *MAPRE2* KO and isogenic control (CTRL) hiPSC-CMs. A constant ohmic current was injected to set the membrane potential just before the APs at approximately -80 mV to overcome the depolarized state of the hiPSC-CMs (Methods). Inset shows the first derivative of V_{max} . **e**, Average V_{max} and APD at 30% and 90% repolarization (APD₃₀ and APD₉₀, respectively) in CTRL and *MAPRE2* KO hiPSC-CMs. V_{max} ($P = 8.1 \times 10^{-6}$), APD₃₀ ($P = 4.8 \times 10^{-6}$) and APD₉₀ ($P = 6.0 \times 10^{-7}$) differed significantly between CTRL and *MAPRE2* KO hiPSC-CM (** $P < 0.01$; unpaired two-tailed Student's *t*-test). Maximal diastolic potential (-56.4 ± 1.5 mV (CTRL) versus -55.6 ± 1.6 mV (*MAPRE2* KO)) and AP amplitude (114.8 ± 6.7 mV (CTRL) versus 121.8 ± 4.2 mV (*MAPRE2* KO)) did not differ significantly between CTRL ($n = 15$) and *MAPRE2* KO ($n = 12$) hiPSC-CMs (unpaired two-tailed Student's *t*-test). **f**, (Left) Average current-voltage relationships of the I_{Na} . (Right) Average repolarizing $I_{outward}$ in CTRL and *MAPRE2* KO hiPSC-CMs. Insets show voltage protocol used. * $P < 0.05$, ** $P < 0.01$ versus CTRL (two-way analysis of variance). Results are expressed as mean \pm s.e.m. Numbers in the bar graph refer to the number of hearts or cells studied.

with lower *MAPRE2* expression in left ventricular tissue compared with the non-risk allele. *MAPRE2* encodes the microtubule plus-end binding protein EB2, a regulator of microtubule organization¹⁷. Whereas effects on transcription factor expression and ion-channel patterning are established molecular mechanisms associated with BrS susceptibility^{3,13}, mechanisms involving microtubule function and ion-channel trafficking, as suggested by the association signal near *MAPRE2*, have not yet been explored. We therefore generated loss-of-function mutants (knockout; KO) using CRISPR-Cas9 in both zebrafish (Supplementary Fig. 7) and human induced pluripotent stem cell-derived cardiomyocytes (hiPSC-CMs) (Supplementary Fig. 8) to study the role of *MAPRE2* in cardiac electrophysiology. Using optical mapping, we observed a significantly lower conduction velocity (CV) and action potential upstroke velocity (V_{max}) in zebrafish hearts isolated from *mapre2* KO compared with control (CTRL) larvae (Fig. 2a,b). Similarly,

V_{max} observed in single *MAPRE2* KO hiPSC-CMs was lower than isogenic control hiPSC-CMs measured using manual patch-clamp (Fig. 2d,e). The lower V_{max} observed in both mutant zebrafish and hiPSC-CMs suggested lower I_{Na} . This was confirmed by automated patch-clamp measurements, which demonstrated ~50% less I_{Na} density in *MAPRE2* KO compared with control hiPSC-CMs (Fig. 2f, left). Additionally, a small positive shift in the voltage dependency of activation was observed, although voltage dependency of inactivation and recovery from inactivation were not different between control and KO cells (Extended Data Fig. 3a–c). Whereas no repolarization abnormalities were observed in intact *mapre2* KO zebrafish hearts (Fig. 2c), significant action potential duration (APD) prolongation was observed in single *MAPRE2* KO hiPSC-CMs (Fig. 2d,e). This APD prolongation may be explained by the significantly lower repolarizing outward current ($I_{outward}$) amplitude in the KO hiPSC-CMs (Fig. 2f, right), although the voltage dependency of

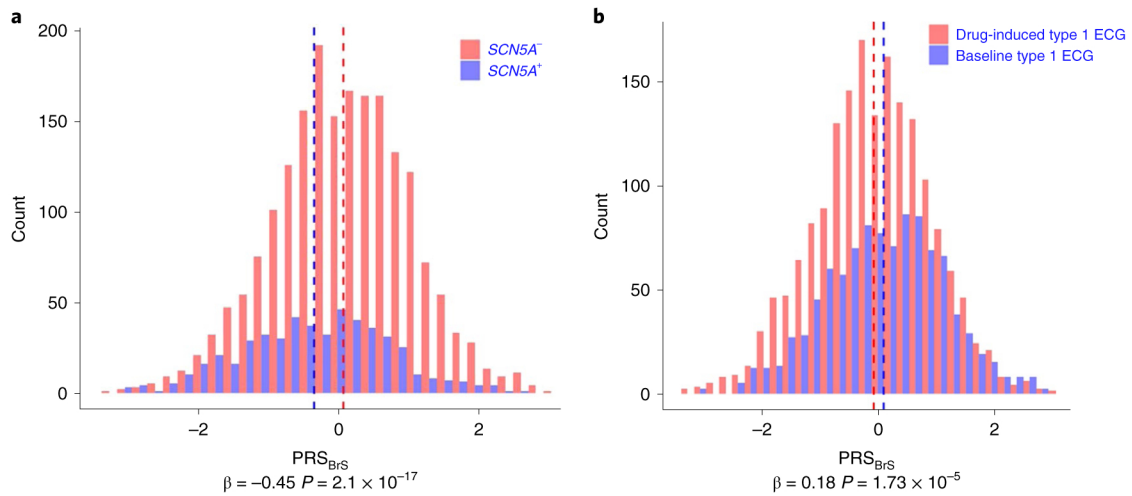


Fig. 3 | Distribution of PRS_{BrS} in specific patient subgroups. **a**, Histograms displaying PRS_{BrS} distribution in BrS cases carrying a rare pathogenic or likely pathogenic variant in *SCN5A* ($SCN5A^+$; blue) compared with BrS cases without such variants ($SCN5A^-$; red). **b**, Histograms displaying PRS_{BrS} distribution in BrS cases presenting with a spontaneous type 1 BrS ECG (blue) compared with those presenting with a type 1 BrS ECG only after sodium channel blocker challenge (drug-induced; red). PRS_{BrS} was calculated per individual on the basis of the 21 BrS risk alleles and their corresponding effect sizes. Results were obtained after logistic regression, two-sided P value not corrected for multiple testing. Reported P values refer to the difference in PRS_{BrS} units between two groups. Dashed lines showing the mean PRS_{BrS} for each group.

activation was unchanged (Extended Data Fig. 3d,e). Together with the multiple levels of evidence that implicate conduction slowing and decreased I_{Na} in the pathogenesis of BrS, and previous work linking end binding proteins to ion-channel targeting to the plasma membrane²⁴, our data suggest that modulation of microtubule function and subsequent alterations in ion-channel trafficking may be a new molecular mechanism contributing to BrS. Future work is needed to address the underlying molecular mechanisms and provide insight into the ion channels that underlie the observed abnormalities in repolarization, although a role for prolonged repolarization is not reconcilable with current hypotheses on BrS pathogenesis²⁵.

To further explore the genetic architecture of BrS in specific patient subgroups as well as the association of common variants in aggregate with disease severity, we calculated a polygenic risk score (PRS_{BrS}) per individual on the basis of the 21 risk alleles and their corresponding effect sizes. Of the 2,469 study participants tested, 454 (18.4%) carried a rare pathogenic or likely pathogenic variant in *SCN5A* ($SCN5A^+$). $SCN5A^+$ cases had a lower mean PRS_{BrS} compared with cases without such variants ($SCN5A^-$) (8.8 ± 1.1 versus 9.3 ± 1.0 ; $P = 2.1 \times 10^{-17}$; Fig. 3a), suggesting a higher burden of BrS-associated common variants in $SCN5A^+$ patients, as similarly shown in other heritable diseases^{26,27}. Using LDSC, we observed a strong genome-wide correlation between the genetic contributors in $SCN5A^+$ and $SCN5A^-$ patient subgroups ($r_g = 0.82$; s.e. = 0.2), suggesting the involvement of the same risk alleles. Of 2,367 BrS cases with complete data, 228 had a life-threatening arrhythmic event (LAE) at diagnosis or during follow-up (median age at last follow-up was 50.0 years, interquartile range 39.5–60.7). Although $SCN5A^+$ cases had a higher risk for LAE compared with $SCN5A^-$ cases (hazard ratio 1.87; 95% confidence intervals (CI) 1.37–2.55; $P = 8.1 \times 10^{-5}$; Supplementary Table 9), PRS_{BrS} was not significantly associated with LAE in BrS cases ($P = 0.30$, Supplementary Fig. 9). However, PRS_{BrS} was significantly higher in BrS cases that presented with a spontaneous type 1 BrS ECG compared with those with a type 1 BrS ECG after sodium channel blocker challenge (9.3 ± 1.1 versus 9.1 ± 1.1 ; $P = 1.7 \times 10^{-5}$; Fig. 3b), an effect that seemed more pronounced in the subgroup of $SCN5A^-$ cases (9.2 ± 1.0 versus 9.5 ± 1.1 ; $P = 3.5 \times 10^{-8}$; Extended Data Fig. 4). These data support the concept that disease susceptibility in different individuals

relies upon varying contributions of multiple factors, including both rare and common genetic variations and exposure to sodium channel blockade.

To explore the genetic relationship of BrS with other traits, we performed a phenome-wide association study (PheWAS) in the UK Biobank using PRS_{BrS} , applying Bonferroni correction ($P < 7 \times 10^{-4}$) to define statistical significance (Fig. 4a and Supplementary Tables 10–12). PRS_{BrS} was associated with a greater risk for atrioventricular conduction disorders ($P = 1.5 \times 10^{-9}$; OR = 1.16 (1.10–1.21) per s.d. increase), as well as longer ECG activation/conduction times reflected in the P-wave duration ($P = 5.3 \times 10^{-9}$; $\beta = 0.76$ ms, s.e. = 0.13), PQ interval duration ($P = 1.9 \times 10^{-45}$; $\beta = 2.70$ ms, s.e. = 0.19) and QRS-complex (QRS) duration ($P = 4.2 \times 10^{-55}$; $\beta = 1.23$ ms, s.e. = 0.08). This underscores the important role of conduction slowing in the pathogenesis of BrS, and is further supported by a significant positive genome-wide correlation between BrS and QRS duration²⁸ ($r_g = 0.44$, $P = 1 \times 10^{-8}$; Supplementary Table 13). By contrast, PRS_{BrS} was negatively associated with the QT interval duration ($P = 4.8 \times 10^{-16}$; $\beta = -1.56$ ms, s.e. = 0.19), consistent with suggestions of higher cardiomyocyte phase 1 repolarizing drive in BrS^{13,25}. PRS_{BrS} was also negatively associated with the occurrence of atrial fibrillation (AF) or flutter ($P = 6.2 \times 10^{-13}$; OR = 0.94 (0.92–0.95)). The effects of each of the 21 BrS risk alleles in previously published GWAS of PQ²⁹, QRS²⁸, QT³⁰ and AF³¹ are generally concordant with the aggregate effect of those alleles (PRS_{BrS}) in the PheWAS (Fig. 4b, Extended Data Fig. 5 and Supplementary Tables 14–17). One exception is the BrS risk allele near *MYO18B* (rs133902-T), which was also associated with greater risk for AF ($P = 9 \times 10^{-10}$ in Nielsen et al.³², and $P = 1 \times 10^{-7}$ in Roselli et al.³¹; Extended Data Fig. 5). This suggests that although changes in CV through sodium channel expression effects modulate risk for AF and BrS in opposite directions, some disease mechanisms such as those involving structural proteins (for example, *MYO18B*) may be shared in both arrhythmias, with concordant effects. We also observed new associations of PRS_{BrS} with nonelectrical phenotypes, namely body mass index (log-transformed; $P = 6.2 \times 10^{-6}$; $\beta = 0.0012$, s.e. = 0.0003) and systolic blood pressure ($P = 4.3 \times 10^{-5}$; $\beta = 0.12$ mmHg, s.e. = 0.03; Supplementary Table 12). Of note, a recent study identified a modulatory effect of hypertension in cardiac sodium channel disease³³. Lastly, a lookup of loci

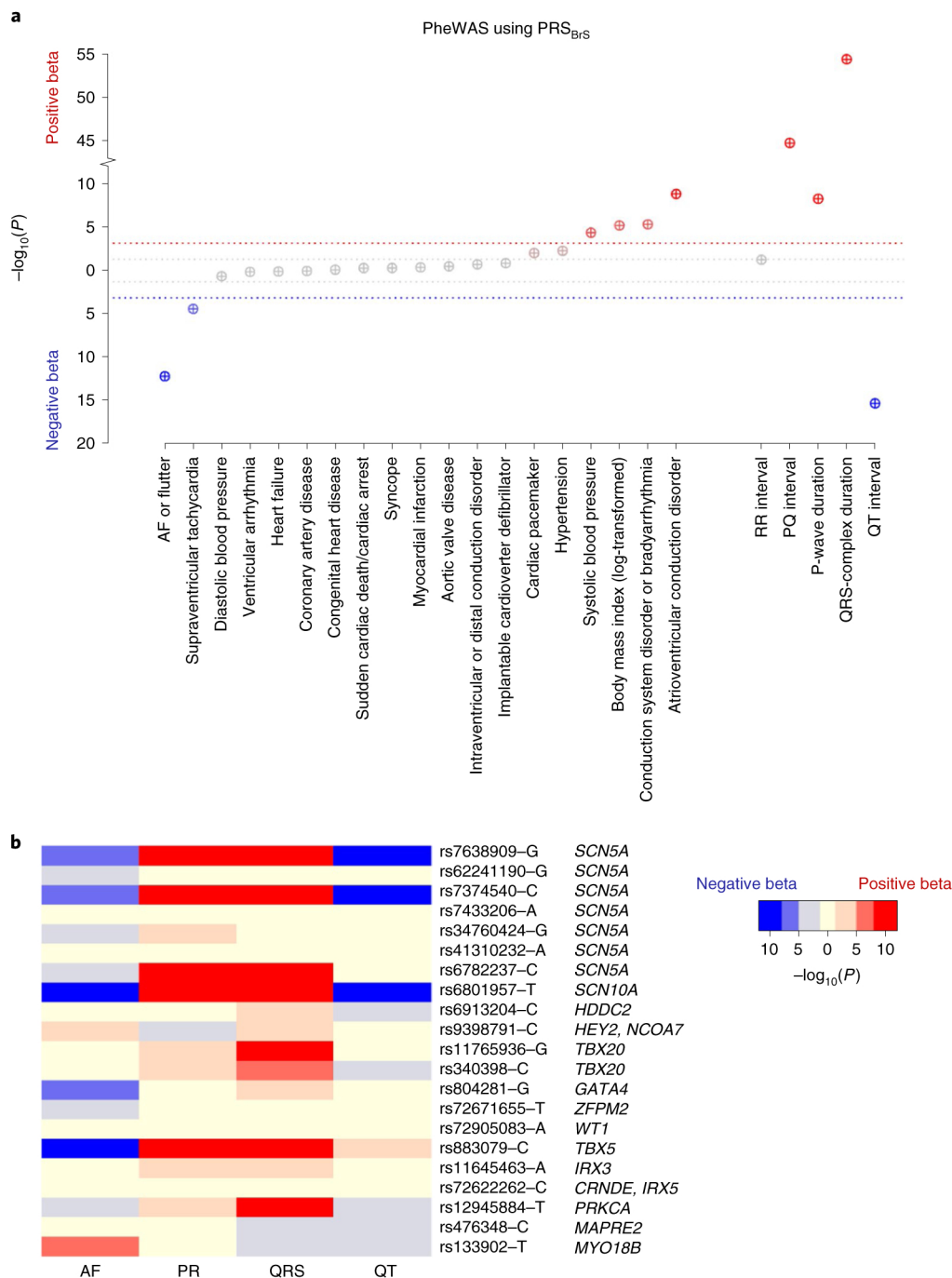


Fig. 4 | Associations between polygenic susceptibility to BrS and common cardiovascular diseases and traits. a, Results of the PheWAS for the PRS_{BrS} among individuals of European ancestry from the UK Biobank. Phenotypes significantly associated with PRS_{BrS} and phenotypes relevant to the heart are shown on the x axis (five electrocardiographic traits are depicted on the right of the plot); the P values from multiple regression are depicted on the y axis. Red circles indicate that polygenic predisposition to BrS is associated with a positive beta (for example, increased risk of the condition or higher value for continuous traits), whereas blue circles indicate that polygenic predisposition to BrS is associated with a negative beta (for example, decreased risk of the condition or lower value). We set the significance threshold to $P < 0.0007$ after Bonferroni correction ($P < 0.05/70$), shown as dotted colored lines. The gray dotted lines indicate the nominal significance threshold ($P < 0.05$). The complete PheWAS results are shown in Supplementary Tables 11 and 12 for dichotomous and continuous traits, respectively. **b,** Heat-map of associations between BrS risk alleles and AF/flutter, PR, QRS and QT from previously published GWAS^{28–31}. The complete PheWAS results are shown in Supplementary Tables 14–17. Each row represents an independent BrS risk allele, whereas each column represents a phenotype. Red indicates that the BrS risk allele (or a proxy with $r^2 > 0.8$) is associated with higher risk of AF or prolongation of the electrocardiographic interval; blue indicates that the BrS risk increasing allele is associated with lower risk of AF or shortening of the interval. The darkest red and blue colors represent conventional genome-wide significance in the published GWAS ($P < 5 \times 10^{-8}$).

previously associated with ECG traits and AF identified nine additional new loci associated with BrS at a Bonferroni-corrected P value $< 1.9 \times 10^{-4}$ (Supplementary Table 18).

In conclusion, several important findings emerge from this work. First, we identified a total of 12 loci (10 new) associated with BrS, a rare disease and a significant cause of sudden cardiac death in young

adults. Three of these loci harbor multiple association signals. Second, the eight independent association signals at the *SCN5A*–*SCN10A* locus highlight the primacy of reduced sodium channel function in BrS susceptibility, whereas the eight loci harboring cardiac transcription factor genes point to transcriptional regulation as a key feature of BrS pathogenesis. Third, functional studies of *MAPRE2* support a new mechanism of $\text{Na}_v1.5$ modulation via the microtubule network in BrS pathogenesis. Fourth, analyses using the UK Biobank highlight a genetic overlap between the BrS and cardiac electrical traits and common disorders in the general population. Finally, PRS analyses support the concept that disease threshold in different individuals with BrS is reached by varying contributions of rare *SCN5A* variants, common risk alleles and sodium channel blockade. Taken together, these findings broaden our understanding of the genetic architecture of BrS and provide new insights into its molecular underpinnings.

References

- Brugada, P. & Brugada, J. Right bundle branch block, persistent ST segment elevation and sudden cardiac death: a distinct clinical and electrocardiographic syndrome. A multicenter report. *J. Am. Coll. Cardiol.* **20**, 1391–1396 (1992).
- Priori, S. G. et al. 2015 ESC Guidelines for the management of patients with ventricular arrhythmias and the prevention of sudden cardiac death: The Task Force for the Management of Patients with Ventricular Arrhythmias and the Prevention of Sudden Cardiac Death of the European Society of Cardiology (ESC). Endorsed by: Association for European Paediatric and Congenital Cardiology (AEPC). *Eur. Heart J.* **36**, 2793–2867 (2015).
- Chen, Q. et al. Genetic basis and molecular mechanism for idiopathic ventricular fibrillation. *Nature* **392**, 293–296 (1998).
- Le Scouarnec, S. et al. Testing the burden of rare variation in arrhythmia-susceptibility genes provides new insights into molecular diagnosis for Brugada syndrome. *Hum. Mol. Genet.* **24**, 2757–2763 (2015).
- Bezzina, C. R. et al. Common variants at *SCN5A*–*SCN10A* and *HEY2* are associated with Brugada syndrome, a rare disease with high risk of sudden cardiac death. *Nat. Genet.* **45**, 1044–1049 (2013).
- Bulik-Sullivan, B. K. et al. LD Score regression distinguishes confounding from polygenicity in genome-wide association studies. *Nat. Genet.* **47**, 291–295 (2015).
- Yang, J. et al. Common SNPs explain a large proportion of the heritability for human height. *Nat. Genet.* **42**, 565–569 (2010).
- Mizusawa, Y. & Wilde, A. A. M. Brugada syndrome. *Circ. Arrhythm. Electrophysiol.* **5**, 606–616 (2012).
- van den Boogaard, M. et al. A common genetic variant within *SCN10A* modulates cardiac *SCN5A* expression. *J. Clin. Invest.* **124**, 1844–1852 (2014).
- van Eif, V. W. W., Devalla, H. D., Boink, G. J. J. & Christoffels, V. M. Transcriptional regulation of the cardiac conduction system. *Nat. Rev. Cardiol.* **15**, 617–630 (2018).
- Gaborit, N. et al. Cooperative and antagonistic roles for *Irx3* and *Irx5* in cardiac morphogenesis and postnatal physiology. *Development* **139**, 4007–4019 (2012).
- Shen, T. et al. *Tbx20* regulates a genetic program essential to adult mouse cardiomyocyte function. *J. Clin. Invest.* **121**, 4640–4654 (2011).
- Veerman, C. C. et al. The Brugada syndrome susceptibility gene *HEY2* modulates cardiac transmural ion channel patterning and electrical heterogeneity. *Circ. Res.* **121**, 537–548 (2017).
- Tarradas, A. et al. Transcriptional regulation of the sodium channel gene (*SCN5A*) by *GATA4* in human heart. *J. Mol. Cell. Cardiol.* **102**, 74–82 (2017).
- Arnolds, D. E. et al. *TBX5* drives *Scn5a* expression to regulate cardiac conduction system function. *J. Clin. Invest.* **122**, 2509–2518 (2012).
- Braz, J. C. et al. PKC- α regulates cardiac contractility and propensity toward heart failure. *Nat. Med.* **10**, 248–254 (2004).
- Goldspink, D. A. et al. The microtubule end-binding protein EB2 is a central regulator of microtubule reorganisation in apico-basal epithelial differentiation. *J. Cell. Sci.* **126**, 4000–4014 (2013).
- Ajima, R. et al. Deficiency of *Myo18B* in mice results in embryonic lethality with cardiac myofibrillar aberrations. *Genes Cells* **13**, 987–999 (2008).
- Gusev, A. et al. Integrative approaches for large-scale transcriptome-wide association studies. *Nat. Genet.* **48**, 245–252 (2016).
- GTEX Consortium et al. Genetic effects on gene expression across human tissues. *Nature* **550**, 204–213 (2017).
- de Leeuw, C. A., Mooij, J. M., Heskes, T. & Posthuma, D. MAGMA: generalized gene-set analysis of GWAS data. *PLoS Comput. Biol.* **11**, e1004219 (2015).
- Finucane, H. K. et al. Heritability enrichment of specifically expressed genes identifies disease-relevant tissues and cell types. *Nat. Genet.* **50**, 621–629 (2018).
- Iotchkova, V. et al. GARFIELD classifies disease-relevant genomic features through integration of functional annotations with association signals. *Nat. Genet.* **51**, 343–353 (2019).
- Gu, C. et al. The microtubule plus-end tracking protein EB1 is required for Kv1 voltage-gated K^+ channel axonal targeting. *Neuron* **52**, 803–816 (2006).
- Wilde, A. A. M. et al. The pathophysiological mechanism underlying Brugada syndrome: depolarization versus repolarization. *J. Mol. Cell. Cardiol.* **49**, 543–553 (2010).
- Talmud, P. J. et al. Use of low-density lipoprotein cholesterol gene score to distinguish patients with polygenic and monogenic familial hypercholesterolaemia: a case-control study. *Lancet* **381**, 1293–1301 (2013).
- Lahrouchi, N. et al. Transethnic genome-wide association study provides insights in the genetic architecture and heritability of long QT syndrome. *Circulation* **142**, 324–338 (2020).
- Sotoodehnia, N. et al. Common variants in 22 loci are associated with QRS duration and cardiac ventricular conduction. *Nat. Genet.* **42**, 1068–1076 (2010).
- van Setten, J. et al. PR interval genome-wide association meta-analysis identifies 50 loci associated with atrial and atrioventricular electrical activity. *Nat. Commun.* **9**, 2904 (2018).
- Arking, D. E. et al. Genetic association study of QT interval highlights role for calcium signaling pathways in myocardial repolarization. *Nat. Genet.* **46**, 826–836 (2014).
- Roselli, C. et al. Multi-ethnic genome-wide association study for atrial fibrillation. *Nat. Genet.* **50**, 1225–1233 (2018).
- Nielsen, J. B. et al. Biobank-driven genomic discovery yields new insight into atrial fibrillation biology. *Nat. Genet.* **50**, 1234–1239 (2018).
- Rivaud, M. R. et al. A common co-morbidity modulates disease expression and treatment efficacy in inherited cardiac sodium channelopathy. *Eur. Heart J.* **39**, 2898–2907 (2018).

Julien Barc^{1,2,108}✉, Rafik Tadros^{3,4,108}, Charlotte Glinge^{3,5,108}, David Y. Chiang^{6,108}, Mariam Jouni^{7,108}, Floriane Simonet^{1,108}, Sean J. Jurgens⁸, Manon Baudic¹, Michele Nicastro³, Franck Potet⁷, Joost A. Offerhaus³, Roddy Walsh³, Seung Hoan Choi⁸, Arie O. Verkerk^{3,9}, Yuka Mizusawa^{2,3}, Soraya Anyas¹, Damien Minois¹, Marine Arnaud¹, Josselin Duchateau^{10,11,12,13}, Yanushi D. Wijeyeratne^{2,14,15}, Alison Muir¹⁶, Michael Papadakis^{14,15}, Silvia Castelletti¹⁷, Margherita Torchio¹⁸, Cristina Gil Ortuño¹⁹, Javier Lacunza²⁰, Daniela F. Giachino^{21,22}, Natascia Cerrato²³, Raphaël P. Martins²⁴, Oscar Campuzano^{25,26,27,28}, Sonia Van Dooren^{2,29}, Aurélie Thollet¹, Florence Kyndt¹, Andrea Mazzanti^{2,30}, Nicolas Clémenty³¹, Arnaud Bisson³¹,

Anniek Corveleyn³², Birgit Stallmeyer³³, Sven Dittmann³³, Johan Saenen³⁴, Antoine Noël³⁵, Shohreh Honarbakhsh³⁶, Boris Rudic^{37,38}, Halim Marzak³⁹, Matthew K. Rowe⁴⁰, Claire Federspiel⁴¹, Sophie Le Page⁴², Leslie Placide⁴³, Antoine Milhem⁴⁴, Hector Barajas-Martinez⁴⁵, Britt-Maria Beckmann^{46,47}, Ingrid P. Krapels⁴⁸, Johannes Steinfurt⁴⁹, Bo Gregers Winkel^{2,5}, Reza Jabbari^{2,5}, Moore B. Shoemaker⁵⁰, Bas J. Boukens⁹, Doris Škorić-Milosavljević³, Hennie Bikker^{2,51}, Federico C. Manevy³, Peter Lichtner⁵², Marta Ribasés⁵³, Thomas Meitinger⁵², Martina Müller-Nurasyid^{54,55,56,57}, KORA-Study Group*, Jan H. Veldink⁵⁸, Leonard H. van den Berg⁵⁸, Philip Van Damme⁵⁹, Daniele Cusi⁶⁰, Chiara Lanzani⁶¹, Sidwell Rigade¹, Eric Charpentier^{1,62}, Estelle Baron¹, Stéphanie Bonnaud^{1,62}, Simon Lecointe¹, Audrey Donnat^{1,62}, Hervé Le Marec¹, Stéphanie Chatel¹, Matilde Karakachoff¹, Stéphane Bézieau¹, Barry London⁶³, Jacob Tfelt-Hansen^{2,5,64}, Dan Roden^{65,66,67}, Katja E. Odening^{49,68}, Marina Cerrone⁶⁹, Larry A. Chinitz⁶⁹, Paul G. Volders⁷⁰, Maarten P. van de Berg⁷¹, Gabriel Laurent⁷², Laurence Faivre⁷³, Charles Antzelevitch⁴⁵, Stefan Käbb^{2,46,74}, Alain Al Arnaout⁴⁴, Jean-Marc Dupuis⁴², Jean-Luc Pasquie⁷⁵, Olivier Billon⁴¹, Jason D. Roberts⁴⁰, Laurence Jesel^{39,76}, Martin Borggrefe^{37,38}, Pier D. Lambiase^{36,77}, Jacques Mansourati³⁵, Bart Loeys⁷⁸, Antoine Leenhardt^{2,79}, Pascale Guicheney^{80,81}, Philippe Maury⁸², Eric Schulze-Bahr^{2,33}, Tomas Robyns^{2,83,84}, Jeroen Breckpot^{2,32}, Dominique Babuty³¹, Silvia G. Priori^{2,30}, Carlo Napolitano^{2,30}, Nantes Referral Center for inherited cardiac arrhythmia*, Carlo de Asmundis^{2,27,85,86}, Pedro Brugada⁸⁷, Ramon Brugada⁸⁸, Elena Arbelo⁸⁹, Josep Brugada⁹⁰, Philippe Mabo²⁴, Nathalie Behar²⁴, Carla Giustetto²³, Maria Sabater Molina¹⁹, Juan R. Gimeno^{2,20}, Can Hasdemir⁹¹, Peter J. Schwartz^{2,17,18}, Lia Crotti^{2,17,18,92,93}, Pascal P. McKeown¹⁶, Sanjay Sharma^{14,15}, Elijah R. Behr^{2,14,15}, Michel Haissaguerre^{10,11,12,13}, Frédéric Sacher^{10,11,12,13}, Caroline Rooryck^{94,95}, Hanno L. Tan^{3,96}, Carol A. Remme³, Pieter G. Postema^{2,3}, Mario Delmar⁹⁷, Patrick T. Ellinor⁹⁸, Steven A. Lubitz⁹⁸, Jean-Baptiste Gourraud^{1,2}, Michael W. Tanck⁹⁹, Alfred L. George Jr.^{7,100}, Calum A. MacRae¹⁰¹, Paul W. Burridge^{7,100}, Christian Dina¹, Vincent Probst^{1,2,108}, Arthur A. Wilde^{2,3,108}, Jean-Jacques Schott^{1,2,108}, Richard Redon^{1,2,108} and Connie R. Bezzina^{2,3,108} ✉

¹Université de Nantes, CHU Nantes, CNRS, INSERM, l'institut du thorax, Nantes, France. ²European Reference Network for Rare and Low Prevalence Complex Diseases of the Heart: ERN GUARD-Heart, <http://guardheart.ern-net.eu>. ³Department of Clinical and Experimental Cardiology, Heart Centre, Amsterdam Cardiovascular Sciences, Amsterdam UMC, University of Amsterdam, Amsterdam, The Netherlands. ⁴Department of Medicine, Cardiovascular Genetics Center, Montreal Heart Institute and Faculty of Medicine, Université de Montréal, Montreal, Quebec, Canada. ⁵The Department of Cardiology, The Heart Centre, Copenhagen University Hospital, Rigshospitalet, Copenhagen, Denmark. ⁶Medicine, Cardiovascular Medicine, Brigham and Women's Hospital, Boston, MA, USA. ⁷Department of Pharmacology, Northwestern University Feinberg School of Medicine, Chicago, IL, USA. ⁸The Broad Institute of MIT and Harvard, Cambridge, MA, USA. ⁹Department of Medical Biology, University of Amsterdam, Amsterdam University Medical Center, Amsterdam, The Netherlands. ¹⁰IHU Liryc, Electrophysiology and Heart Modeling Institute, fondation Bordeaux Université, Pessac-Bordeaux, France. ¹¹Université Bordeaux, Centre de recherche Cardio-Thoracique de Bordeaux, Bordeaux, France. ¹²INSERM, Centre de recherche Cardio-Thoracique de Bordeaux, Bordeaux, France. ¹³Electrophysiology and Ablation Unit, Bordeaux University Hospital (CHU), Pessac, France. ¹⁴Molecular and Clinical Sciences Research Institute, St. George's, University of London, London, UK. ¹⁵Cardiology Clinical Academic Group, St. George's University Hospitals' NHS Foundation Trust, London, UK. ¹⁶Cardiology, Belfast Health and Social Care Trust and Queen's University Belfast, Belfast, UK. ¹⁷Center for Cardiac Arrhythmias of Genetic Origin, Istituto Auxologico Italiano IRCCS, Milan, Italy. ¹⁸Laboratory of Cardiovascular Genetics, Istituto Auxologico Italiano IRCCS, Cusano Milanino, Italy. ¹⁹Cardiogenetic, Unidad de Cardiopatías Familiares, Instituto Murciano de Investigación Biosanitaria, Universidad de Murcia, Murcia, Spain. ²⁰Cardiology, Unidad de Cardiopatías Familiares, Hospital Universitario Virgen de la Arrixaca, Universidad de Murcia, Murcia, Spain. ²¹Clinical and Biological Sciences, Medical Genetics, University of Torino, Orbassano, Italy. ²²Medical Genetics, San Luigi Gonzaga University Hospital, Orbassano, Italy. ²³Medical Sciences, Cardiology, University of Torino, Torino, Italy. ²⁴Cardiologie et Maladies vasculaires, Université Rennes 1 - CHU Rennes, Rennes, France. ²⁵Cardiovascular Genetics Center, University of Girona-IDIBGI, Girona, Spain. ²⁶Medical Science Department, University of Girona, Girona, Spain. ²⁷Centro de Investigación Biomédica en Red de Enfermedades Cardiovasculares (CIBERCV), Madrid, Spain. ²⁸Biochemistry and Molecular Genetics Department, Hospital Clinic, University of Barcelona-IDIBAPS, Barcelona, Spain. ²⁹Centre for Medical Genetics, research group Reproduction and Genetics, research cluster Reproduction, Genetics and Regenerative Medicine, Vrije Universiteit Brussel (VUB), Universitair Ziekenhuis Brussel (UZ Brussel), Brussels, Belgium. ³⁰Molecular Cardiology, ICS Maugeri, IRCCS and Department of Molecular Medicine, University of Pavia, Pavia, Italy. ³¹Department of Cardiology, CHU Tours, Tours, France. ³²Department of Human Genetics, Catholic University Leuven, Leuven, Belgium. ³³University Hospital Münster, Institute for Genetics of Heart Diseases (IfGH), Münster, Germany. ³⁴Cardiology, Electrophysiology - Cardiogenetics, University of Antwerp/Antwerp University Hospital, Edegem, Belgium. ³⁵Department of Cardiology, University Hospital of Brest, Brest, France. ³⁶Cardiology, Medicine, Barts Heart Centre, London, UK. ³⁷Department 1st of Medicine, Cardiology, University Medical Center Mannheim, Mannheim, Germany. ³⁸German Center for Cardiovascular

Research (DZHK), Mannheim, Germany. ³⁹Department of Cardiology, University Hospital of Strasbourg, Strasbourg, France. ⁴⁰Medicine, Cardiology, Western University, London, Ontario, Canada. ⁴¹Department of Cardiovascular Medicine, Vendée Hospital, Service de Cardiologie, La Roche sur Yon, France. ⁴²Service de cardiologie, CHU Angers, Angers, France. ⁴³Department of Cardiology, CHU Montpellier, Montpellier, France. ⁴⁴Department of Cardiology, CH La Rochelle, La Rochelle, France. ⁴⁵Lankenau Institute for Medical Research, Wynnewood, PA, USA. ⁴⁶Department of Medicine I, University Hospital, LMU Munich, Munich, Germany. ⁴⁷University Hospital of the Johann Wolfgang Goethe University Frankfurt, Institute of Legal Medicine, Frankfurt, Germany. ⁴⁸Department of Clinical Genetics, Maastricht University Medical Center, Maastricht, The Netherlands. ⁴⁹Department of Cardiology and Angiology I, Heart Center, University Freiburg, Freiburg, Germany. ⁵⁰Medicine, Cardiology, Vanderbilt University Medical Center, Nashville, TN, USA. ⁵¹Genome Diagnostics Laboratory, Clinical Genetics, Amsterdam UMC, Amsterdam, The Netherlands. ⁵²Institute of Human Genetics, Helmholtz Zentrum München, Neuherberg, Germany. ⁵³Psychiatric Genetics Unit, Institute Vall d'Hebron Research (VHIR), Universitat Autònoma de Barcelona, Barcelona, Spain. ⁵⁴Institute of Genetic Epidemiology, Helmholtz Zentrum München - German Research Center for Environmental Health, Neuherberg, Germany. ⁵⁵IBE, LMU Munich, Munich, Germany. ⁵⁶Institute of Medical Biostatistics, Epidemiology and Informatics (IMBEI), University Medical Center, Johannes Gutenberg University, Mainz, Germany. ⁵⁷Department of Internal Medicine I (Cardiology), Hospital of the Ludwig-Maximilians-University (LMU) Munich, Munich, Germany. ⁵⁸Department of Neurology, UMC Utrecht Brain Center, University Medical Center Utrecht, Utrecht University, Utrecht, The Netherlands. ⁵⁹Neurology Department University Hospital Leuven, Neuroscience Department KU Leuven, Center for Brain & Disease Research VIB, Leuven, Belgium. ⁶⁰Scientific Unit, Bio4Dreams - Business Nursery for Life Sciences, Milan, Italy. ⁶¹Nephrology, Genomics of Renal Diseases and Hypertension Unit, Università Vita Salute San Raffaele, Milan, Italy. ⁶²Université de Nantes, CHU Nantes, Inserm, CNRS, SFR Santé, Inserm UMS 016, CNRS UMS 3556, Nantes, France. ⁶³Department of Internal Medicine, Division of Cardiovascular Medicine, Abboud Cardiovascular Research Center, University of Iowa Carver College of Medicine, Iowa City, IA, USA. ⁶⁴Department of Forensic Medicine, University of Copenhagen, Copenhagen, Denmark. ⁶⁵Medicine, Clinical Pharmacology, Vanderbilt University Medical Center, Nashville, TN, USA. ⁶⁶Medicine, Pharmacology, Vanderbilt University Medical Center, Nashville, TN, USA. ⁶⁷Medicine, Biomedical Informatics, Vanderbilt University Medical Center, Nashville, TN, USA. ⁶⁸Department of Cardiology, Translational Cardiology, University Hospital Bern, Bern, Switzerland. ⁶⁹Medicine, Leon H. Charney Division of Cardiology, Heart Rhythm Center and Cardiovascular Genetics Program, New York University School of Medicine, New York, NY, USA. ⁷⁰Department of Cardiology, CARIM, Maastricht University Medical Center, Maastricht, The Netherlands. ⁷¹Department of Cardiology, University Medical Center Groningen, University of Groningen, Groningen, The Netherlands. ⁷²Cardiology Department, ImVia lab team IFTIM, University Hospital Dijon, Dijon, France. ⁷³Centre de Génétique, FHU TRANSLAD, Dijon, France. ⁷⁴German Center for Cardiovascular Research (DZHK), Partnersite Munich, Munich, Germany. ⁷⁵Department of Cardiology, CNRS UMR9214 - Inserm U1046 - PHYMEDEXP, Université de Montpellier et CHU Montpellier, Montpellier, France. ⁷⁶INSERM 1260 - Regenerative Nanomedicine, University of Strasbourg, Strasbourg, France. ⁷⁷Institute of Cardiovascular Science, UCL, Population Health, UCL, London, UK. ⁷⁸Center for Medical Genetics, Cardiogenetics, University of Antwerp/Antwerp University Hospital, Edegem, Belgium. ⁷⁹Department of Cardiology, Hôpital Bichat, Paris, France. ⁸⁰Sorbonne Université, Paris, France. ⁸¹UMR_S1166, Faculté de médecine, Sorbonne Université, INSERM, Paris, France. ⁸²Service de cardiologie, Hôpital Rangueil, CHU de Toulouse, Toulouse, France. ⁸³Cardiovascular Diseases, University Hospitals Leuven, Leuven, Belgium. ⁸⁴Cardiovascular Sciences, University of Leuven, Leuven, Belgium. ⁸⁵Heart Rhythm Management Center, Postgraduate Program in Cardiac Electrophysiology and Pacing Universitair Ziekenhuis, Brussel-Vrije Universiteit Brussel, ERN Heart Guard Center, Brussels, Belgium. ⁸⁶IDIBAPS, Institut d'Investigació August Pi i Sunyer (IDIBAPS), Barcelona, Spain. ⁸⁷Heart Rhythm Management Center, UZ Brussel-VUB, Brussels, Belgium. ⁸⁸Hospital Trueta, CiberCV, University of Girona, IDIBGI, Girona, Spain, Barcelona, Spain. ⁸⁹Arrhythmia Section, Cardiology Department, Hospital Clínic, Universitat de Barcelona, Barcelona, Spain. ⁹⁰Cardiovascular Institute, Hospital Clínic, University of Barcelona, Barcelona, Spain. ⁹¹Department of Cardiology, Ege University School of Medicine, Bornova, Turkey. ⁹²Department of Cardiovascular, Neural and Metabolic Sciences, San Luca Hospital, Istituto Auxologico Italiano IRCCS, Milan, Italy. ⁹³Department of Medicine and Surgery, University of Milano-Bicocca, Milan, Italy. ⁹⁴CHU Bordeaux, Service de Génétique Médicale, Bordeaux, France. ⁹⁵Université de Bordeaux, Maladies Rares: Génétique et Métabolisme (MRGM), INSERM U1211, Bordeaux, France. ⁹⁶Netherlands Heart Institute, Utrecht, The Netherlands. ⁹⁷Medicine, Cardiology, New York University School of Medicine, New York, NY, USA. ⁹⁸Cardiac Arrhythmia Service and Cardiovascular Research Center, Massachusetts General Hospital and Cardiovascular Disease Initiative, The Broad Institute of MIT and Harvard, Boston, MA, USA. ⁹⁹Clinical Epidemiology, Biostatistics and Bioinformatics, Clinical Methods and Public Health, Amsterdam Public Health, Amsterdam, The Netherlands. ¹⁰⁰Center for Pharmacogenomics, Northwestern University Feinberg School of Medicine, Chicago, IL, USA. ¹⁰¹Medicine, Cardiovascular Medicine, Genetics and Network Medicine, Brigham and Women's Hospital and Harvard Medical School, Boston, MA, USA. ¹⁰⁸These authors contributed equally: Julien Barc, Rafik Tadros, Charlotte Glinge, David Y. Chiang, Mariam Jouni, Floriane Simonet, Vincent Probst, Arthur A. Wilde, Jean-Jacques Schott, Richard Redon, Connie R. Bezzina. *Lists of authors and their affiliations appear at the end of the paper. ⁸²e-mail: julien.barc@univ-nantes.fr; c.r.bezzina@amsterdamumc.nl

KORA-Study Group

Konstantin Strauch^{54,56,102}, Annette Peters¹⁰³, Holger Schulz¹⁰³, Lars Schwettmann¹⁰³, Reiner Leidl¹⁰³ and Margit Heier¹⁰³

¹⁰²Genetic Epidemiology, IBE, Faculty of Medicine, LMU Munich, Munich, Germany. ¹⁰³Institute of Health Economics and Health Care Management, Helmholtz Zentrum München - German Research Center for Environmental Health, Neuherberg, Germany.

Nantes Referral Center for inherited cardiac arrhythmia

Vincent Probst^{1,2,108}, Jean-Baptiste Gourraud^{1,2}, Frédéric Sacher^{10,11,12,13}, Raphaël P. Martins²⁴, Dominique Babuty³¹, Jacques Mansourati³⁵, Jean-Luc Pasquie⁷⁵, Jean-Marc Dupuis⁴², Laurence Jesel^{39,76}, Gabriel Laurent⁷², Olivier Billon⁴¹, Alain Al Arnaout⁴⁴, Pascal Defaye¹⁰⁴, Frédéric Anselme¹⁰⁵, Jean Philippe Darmon¹⁰⁶, François Wiart¹⁰⁷ and Philippe Maury⁸²

¹⁰⁴CHU Grenoble, Service de Cardiologie, Grenoble, France. ¹⁰⁵Cardiology Department, CHU de Rouen, Rouen, France. ¹⁰⁶Cardiology Department, CH de Le Mans, Le Mans, France. ¹⁰⁷Service de cardiologie, CHU de La Réunion, Saint-Denis, Réunion, France.

Methods

Case inclusion and study design. We established an international consortium allowing the inclusion of 2,820 unrelated individuals with BrS from 39 BrS reference centers in 12 countries (Supplementary Table 1). All human participants provided written informed consent, and all studies had received approval from the appropriate ethical review boards (Reporting Summary). The diagnosis of BrS was made according to the 2013 Heart Rhythm Society, European Heart Rhythm Association and Asia Pacific Heart Rhythm Society expert consensus statement³⁴, the 2015 European Society of Cardiology guidelines³⁵ and the 2017 American Heart Association guidelines³⁵. Specifically, cases were included if they had a type 1 BrS ECG, that is, a coved type ST elevation at baseline (spontaneous) or after a drug challenge test, in one or more leads in the right precordial leads V1 and/or V2 in the standard position (fourth intercostal space) or in high positions (second or third intercostal spaces). Diagnostic ECGs were centrally assessed by a cardiac electrophysiologist with expertise in BrS (J.-B.G., Y.M. or R.T.) to ensure the diagnostic ECG criteria were reached. Clinical data collection was performed at each site, including age at diagnosis, presence of a variant in *SCN5A*, presence of a spontaneous type 1 BrS ECG or a type 1 BrS ECG observed after drug challenge, implantable cardioverter–defibrillator implantation, time of occurrence of LAEs, and family history of sudden cardiac death. LAEs were defined as out-of-hospital cardiac arrest or hemodynamically unstable ventricular tachycardia/ventricular fibrillation.

Assessment of the pathogenicity of reported *SCN5A* variants. The *SCN5A* gene had been screened for rare variants in 87.6% of individuals. Pathogenicity of rare variants in *SCN5A* identified in included BrS cases was centrally assessed using the American College of Medical Genetics and Genomics and Association of Molecular Pathology guidelines³⁶, using an adapted version of CardioClassifier³⁷ incorporating a quantitative approach on the basis of case–control analyses, as performed previously in hypertrophic cardiomyopathy genes³, as well as a curated compendium of functional data⁴. Specifically, the following American College of Medical Genetics and Genomics/Association of Molecular Pathology rules were applied:

- PM2/BS1: The PM2 or BS1 rules were activated depending on whether the gnomAD exomes filtering allele frequency was below or above the calculated maximum tolerated allele frequency for BrS. The threshold applied was 2.5×10^{-5} , calculated with <https://www.cardiodb.org/allelefrequencycapp/> using a disease prevalence of 1 in 2,000, allelic heterogeneity of 0.01 and penetrance of 0.10.
- BA1: Filtering allele frequency in gnomAD exomes > 0.001 .
- PVS1: Truncating variants in *SCN5A*, that is frameshift, nonsense, splice donor and splice acceptor variants.
- PS4: Variant is enriched in case cohorts (on the basis of published BrS *SCN5A* compendium³⁸) compared with ExAC population controls (Fisher's exact test, $P < 1.79 \times 10^{-6}$ after multiple testing correction), as applied by CardioClassifier.
- PP3/BS4: Multiple lines of computation evidence support or refute a deleterious effect, as applied by CardioClassifier.
- PM4: A protein length change as a result of an in-frame deletion or insertion in a non-repeat region.
- BP3: In-frame insertion or deletion that falls within a region annotated by repeat masker.
- PS1: Same amino acid change as a previously established pathogenic variant (multiple ClinVar submissions with no conflicting evidence).
- PM5: New missense change at an amino acid residue where a different missense change has previously been established as pathogenic (multiple ClinVar submissions with no conflicting evidence).
- PS1_moderate/PM5_supporting: Known disease-causing variant affecting the same residue in a paralogous protein³⁹, either with the same or a different amino acid substitution, respectively.
- PS3/BS3: Functional evidence showing a deleterious effect (or no deleterious effect) of the variant on the basis of published cellular electrophysiology studies curated by Denham et al.⁴⁰.
- PM1: This rule was applied on the basis of precomputed etiological fraction (EF) values for rare, nontruncating variants as described by Walsh et al.⁴¹. This approach defines the prior probability, as calculated through case–control cohort analysis, that a variant in a particular gene/protein region is pathogenic. The rules applied are PM1_strong (EF ≥ 0.95), PM1_moderate ($0.9 < EF < 0.95$) or PM1_supporting ($0.8 \leq EF < 0.9$). For *SCN5A* variants, this analysis was performed using case data from this study and population data from gnomAD exomes. Protein domains were defined according to the Uniprot (v.207) entry [Q14524](#) with the four transmembrane regions and three interlinker domain regions assessed together as functionally equivalent domains. The PM1_strong rule was applied to the transmembrane regions (amino acid residues 132–410, 718–938, 1,207–1,466, 1,530–1,771) and the PM1_supporting rule was applied to the N-terminus region (residues 1–131).

Rules based on cosegregation of variants with disease in family pedigrees (PP1/BS4) or de novo inheritance with/without confirmed paternity and maternity (PS2/PM6) were not applied.

GWAS analysis design, description of the strata and quality control. Quality control (QC) and case–control association analysis were performed in ten strata (see Supplementary Note for a full description of the ten different strata; Supplementary Table 2) followed by meta-analysis, as described in the following sections. Samples were grouped into strata on the basis of common ancestry (as determined by principal component analysis of genotypic data; Supplementary Fig. 1), same genotyping platform and time of genotyping. To ensure that none of the BrS cases were included in multiple strata, a genotypic relatedness analysis on the basis of identity by state was performed using a linkage disequilibrium (LD) pruned set of SNPs that were overlapping between all strata.

Imputation and association analyses. Genome-wide imputation was performed per stratum using Eagle2 phasing, Minimac3 and the Haplotype Reference Consortium (HRCr1.1) panel implemented on the Michigan Imputation Server v.1.0.2 (ref. ⁴²). After imputation, only SNPs with MAF > 0.01 and a Minimac $R^2 > 0.5$ were taken forward in the association analysis.

The association of alternate allele dosage with BrS was performed for each of the ten strata using a frequentist test in an additive model implemented in SNPTEST (v.2.5.2), correcting for the first six genotypic principal components. The summary results of the ten strata were then combined using an inverse-variance weighted fixed-effect meta-analysis, performing meta-analysis heterogeneity analysis, implemented in METAL (version released on 25 March 2011). SNPs that were missing in four or more of the ten strata, as well as those with a heterogeneity test $P < 10^{-7}$ were excluded.

We sought to uncover additional association signals at BrS loci using conditional analysis. Specifically, for each locus reaching the genome-wide statistical significance threshold ($P < 5 \times 10^{-8}$), a frequentist test implemented in SNPTEST (v.2.5.2) was performed correcting for the first six genotypic principal components and conditioning on the lead SNP at the locus, for each of the ten strata, followed by meta-analysis. If another independent signal reaching genome-wide significance was identified at the locus in the meta-analysis, a second analysis conditioning on the two independent lead SNPs at the locus was then performed. This was repeated until no independent signal reached genome-wide statistical significance.

The results of the case–control meta-analysis are shown in Fig. 1, Table 1 and Supplementary Table 3. Principal component analyses plots of cases and controls in each of the ten GWAS strata are shown in Supplementary Fig. 1. QQ plots of each stratum are reported in Supplementary Fig. 2 and forest plots for all loci reaching $P < 5 \times 10^{-8}$ are shown per stratum and overall (summary) in Supplementary Fig. 3. Stratum-specific odds ratios (OR), 95% CI and P values are based on logistic regression assuming an additive genetic model. Summary OR and 95% CI values are from fixed-effects meta-analysis. Forest plots were generated using the *rmeta* library implemented in the R project (R forestplot).

Analysis of heritability attributable to common variants. We used the generalized restricted maximum likelihood (GREML) approach of GCTA (v.1.92.4 beta)^{43,44} to estimate how much of the variance in BrS susceptibility could be attributed to common genetic variants (SNP-based heritability, h^2_{SNP}). The analysis was performed by stratum, followed by a fixed-effects meta-analysis using the *meta* package in R v.3.6.0. The GSA_TUR stratum was excluded given its small sample size ($n = 300$) where GREML failed. Before heritability analyses, we performed additional stringent postimputation QC as suggested⁴⁵, using hard call genotypes (genotype probability > 0.9) and excluding SNPs with missing rate > 0.01 , MAF < 0.05 , Hardy–Weinberg test $P < 0.05$ and phenotype biased missingness $P < 0.05$, as well as samples with missing rate > 0.01 . Less-stringent QC was used for the GSA_IT stratum to allow for sufficient SNPs to remain for GREML. For each stratum, we generated a genetic relationship matrix and excluded distantly related individuals (proportion IBD > 0.05). We estimated h^2_{SNP} on the liability scale assuming a prevalence ranging from 0.005 to 0.0005 (refs. ^{8,46}) with the first 20 genotypic principal components and sex as covariates. We also estimated h^2_{SNP} attributable to the 12 loci associated with BrS at genome-wide statistical significance. Loci were defined as ± 500 kb from the lead SNP(s) in primary or conditional analyses. The proportion of heritability explained by the 12 loci was calculated by dividing their h^2_{SNP} by the genome-wide h^2_{SNP} . As an alternative to GREML, we also used LDSC (1.0.0) to calculate SNP heritability using the meta-analysis summary statistics, restricted to the ~ 1.2 million HapMap SNPs, using the 1000 Genomes European population as a reference. The results of h^2_{SNP} estimation are shown in Supplementary Table 4.

Locus annotation. Association signals from the meta-analysis were annotated by presence of: (1) (proxy) coding variants; (2) cis-eQTL; (3) cis-splice quantitative trait loci (sQTL); and (4) contact with promoters of nearby genes.

(Proxy) coding variants. We performed a lookup to assess whether the lead SNP or variants in LD with the lead SNP alter the protein-coding region of a gene. An $r^2 \geq 0.6$ was applied, defined using the European subset of the 1000 Genomes Project in LDlink⁴⁷. Protein-altering coding variants were defined as missense, splice site (within two nucleotides of the exon–intron boundary), in-frame deletions/insertions, frameshift and stopgain. Coding variants defined in this way are listed in Supplementary Table 3.

cis-eQTL. For each association signal, we used the left ventricular tissue dataset from the GTEx (accessed December 2019)²⁰ to identify cis-eQTLs. Significance of a variant–gene association was defined using a Bonferroni-corrected P -value threshold, correcting for the number of genes within 1 Mb of the association signal. As such, the P -value thresholds ranged from 5.56×10^{-3} to 1.85×10^{-3} . Significant eQTLs are listed in Supplementary Table 3 and displayed in Supplementary Fig. 4. Significant eQTLs were assessed for colocalization using eCAVIAR⁴⁸ to determine colocalization with the GWAS hit. Heart—Left Ventricle eQTLs from GTEx v.7 were used; eCAVIAR used SNP, eQTL z -scores and LD correlation values to calculate a colocalization posterior probability of a trait GWAS locus and an eQTL. We calculated LD of SNPs 1 Mb on both sides of the SNPs, using European ancestry Heart Rhythm Society samples (dbGaP accession code [phs000428.v2.p2](#)) as a reference. We used the default assumption of two causal SNPs. CLPP for eQTL hits are displayed in Supplementary Table 3.

cis-sQTL. We assessed whether the lead SNP at each locus displayed a cis-sQTL effect by performing a lookup in the left ventricular tissue dataset of GTEx (accessed March 2020)²⁰. Only variants with a significant variant–gene association are reported.

Hi-C. Interaction between associated loci and target regions was assessed using the tissue-specific 3D chromatin interaction (Hi-C) mapping function, incorporated in FUMA⁴⁹. Hi-C data from human left ventricle²⁰ was explored and interactions with an $FDR \leq 10^{-6}$ are reported in Supplementary Fig. 4 and listed in Supplementary Table 3. Target regions including the transcription start site are displayed in bold.

Analysis for enrichment in genes encoding DNA-binding proteins. We used SNPsnap⁵¹ to generate 10,000 sets of 12 SNPs that had characteristics matching the lead SNPs at the non-chromosome 3 BrS loci. We took 12 SNPs because the two lead SNPs at the *TBX20* locus were located close to each other and only one of these was therefore considered. SNPs were matched on the basis of MAF, number of SNPs in LD, distance to nearest gene and number of nearby genes (gene density). Genes listed in gene ontology (GO) term ‘sequence-specific DNA binding’ (GO:0043565) were used as a broad list of genes encoding DNA-binding proteins. Enrichment was assessed by permutation testing across the 10,000 SNP sets to determine the neutral expectation for the number of DNA-binding proteins overlapping or in vicinity of SNPs with characteristics similar to ours, yielding a P value for a one-tailed test. An SNP was considered near a gene encoding a DNA-binding protein if it was within a radius of 300 kb upstream or downstream of any gene on the GO term list.

Genome-wide visualization and annotation. The BrS GWAS summary statistics were uploaded to Functional Mapping and Annotation of GWAS (FUMA)⁴⁹ for visualization and genome-wide analyses. Gene-set and tissue expression analyses were performed using MAGMA⁵² implemented in FUMA. GO gene sets from the Molecular Signatures Database (MSigDB, v.6.2)⁵³ were used for the gene-set analysis, and GTEx (v.8) was used for tissue specificity analysis²⁰. The results of MAGMA gene-set analyses are shown in Supplementary Table 8 and the results of MAGMA tissue-specificity analyses are shown in Supplementary Fig. 5.

We used GARFIELD²³ to correlate the GWAS findings with regulatory or functional annotations and find features relevant to a phenotype of interest. Because our GWAS included only European individuals, we used the original files describing the allele frequencies and linkage disequilibrium from the UK10K data provided in the GARFIELD distribution. We also used the annotation and distance to TSS files provided with the GARFIELD release. The annotations included 1,005 features extracted from ENCODE, GENCODE and Roadmap Epigenomics projects, including genic annotations, chromatin states, histone modifications, DNaseI hypersensitive sites and transcription factor binding sites, among others, in a number of publicly available cell lines. Enrichment P value is determined empirically through a permutation procedure accounting for associated regions structures on the basis of the number of SNPs and mean LD. Because the chromosome 3p region presents a complex structure with a set of SNPs both physically close and highly associated, we also ran the enrichment analysis without this region. Results of GARFIELD functional enrichment analyses are shown in Supplementary Table 7 and Supplementary Fig. 6.

Alternatively, we used stratified LDscore regression⁵⁴ to estimate the contribution to heritability for cell type or tissue-specific elements. In this extended model, the expected SNP association statistic (c^2) is modeled by LDscore as previously and by a binary variable C (for category) which takes value 1 if the SNP falls into the functional category (and 0 otherwise). Multiple regression is applied. We label regions as putatively functional or not for each annotation (function/tissue) using the functional map estimated by the method FUN-v-LDA⁵⁵ for the Roadmap-Epigenomic project. Results from this LDSC enrichment test are shown in Supplementary Table 6.

Transcriptome-wide association study. TWAS was performed using FUSION¹⁹ and eQTL data in cardiac tissues (left ventricle and atrial appendage) from GTEx²⁰. Gene expression weights were calculated using prediction models implemented in FUSION. This includes top1 (that is, the single most significant eQTL-SNP as the predictor), LASSO regression, elastic net regression and

best linear unbiased prediction. SNP data located 500 kb on both sides of the probes were used to obtain expression weights. There were 4,490 and 5,225 genes with significant cis-heritability ($h^2 > 0.05$) for left ventricle and atrial appendage cardiac tissues, respectively, to calculate expression weights. Expression weights were then combined with summary-level results from the meta-analysis to estimate association statistics between gene expression and BrS. Genome-wide significant TWAS genes were considered at $P_{TWAS} < 5.2 \times 10^{-6}$ (Bonferroni = $0.05/4,490 + 5,225$). Significant genes identified by TWAS are listed in Supplementary Table 5.

BrS polygenic score. PRS_{BrS} was derived from the BrS case–control GWAS. All independent lead SNPs reaching the genome-wide significance threshold ($P < 5 \times 10^{-8}$) in either the primary or conditional analyses were included (total of 21 SNPs, Table 1). The score for each individual was calculated by taking the sum of risk allele dosage weighted by the beta coefficient estimated in the GWAS over these SNPs. To assess whether the burden of BrS-associated common variants differs between distinct BrS subgroups, we tested the association between certain subgroups and PRS_{BrS} using linear regression. We performed a total of seven predefined analyses involving PRS_{BrS}: (1) comparison of PRS_{BrS} in SCN5A⁺ versus SCN5A[−] ($n = 1$); (2) association of PRS_{BrS} with LAE in all BrS, SCN5A[−] BrS and SCN5A⁺ BrS ($n = 3$); and (3) association of PRS_{BrS} with the occurrence of type 1 ECG at baseline versus drug-induced in all BrS, SCN5A[−] BrS and SCN5A⁺ BrS ($n = 3$). The Bonferroni-corrected threshold for significance was set to $P < 0.007$ ($0.05/7$). The five first principal components were used as covariates in a sensitivity analysis, and results were similar to the analysis without covariates. These data are presented in Fig. 3 and Extended Data Fig. 4.

Survival analyses. Time to LAEs (defined as out-of-hospital cardiac arrest or hemodynamically unstable ventricular tachycardia/ventricular fibrillation) survival analyses were performed in the BrS cases. Follow-up started at birth and ended at the date of an event, the last visit or the 70th birthday, whichever came first. Cox proportional hazards regression models were first used to assess the association of clinical risk factors with LAE in univariable followed by multivariable models. The adjusted Cox regression multivariable model included sex, SCN5A⁺ and spontaneous type 1 ECG. The proportional hazard assumptions were verified through examination of Schoenfeld residuals plots. For all analyses, a P value < 0.05 was considered statistically significant. All analyses were performed using SAS software, v.9.4 (SAS Institute Inc.), and R v.3.4. Kaplan–Meier curves were created to illustrate the event-free survival within PRS_{BrS} quartiles, and single SNP genotypes and log-rank tests were used to compare the survival curves. The effect of the PRS_{BrS} (continuous) and single SNP genotypes was estimated using Cox proportional hazards regression with adjustment for sex, genotypic PC1–PC6, the presence of a pathogenic or likely pathogenic variant in SCN5A and spontaneous type 1 BrS ECG. All SNP- or PRS_{BrS}-based statistical analyses were performed in three strata separately based on genotypic platform (Affymetrix CEU, PMRA and Illumina GSA) followed by meta-analysis using an inverse-variance weighted fixed-effect model, implemented in METAL (version released on 25 March 2011)⁵⁶. Results from these survival analyses are shown in Supplementary Table 9 and Supplementary Fig. 9.

Pairwise genetic correlation. We performed pairwise genetic correlation between BrS and published GWAS studies of ECG traits (PR²⁹, QRS²⁸ and QT³⁰) and AF^{31,32}, using LDSC (v.1.0.1)^{36,37}. For each GWAS, we first reformatted summary statistics using the ‘munge_sumstats.py’ command, filtering for the HapMap3 SNPs with corresponding alleles using the ‘-merge-alleles w_hm3.snplist’ flag, as recommended. The HapMap3 SNPs were downloaded from https://data.broadinstitute.org/alkesgroup/LDSCORE/w_hm3.snplist.bz2. We then assessed genetic correlation using the ‘ldsc.py -rg’ command and precomputed LD scores from the European 1000 Genomes Project dataset which were downloaded from https://data.broadinstitute.org/alkesgroup/LDSCORE/eur_w_ld_chr.tar.bz2. In the primary analysis, we did not constrain the single-trait and cross-trait LDscore regression intercepts. The results of the genetic correlation analyses are shown in Supplementary Table 13.

PheWAS of PRS_{BrS} in the UK Biobank. The UK Biobank is a large prospective cohort study from the United Kingdom with deep phenotypic and genotypic data on ~500,000 individuals enrolled aged 40–69 (refs. ^{57,58}). Phenotypic data were ascertained from anthropometric measurements, surveys, medical history reviews and electronic health records. Individuals were genotyped using one of two similar custom arrays (UK BiLEVE Axiom Array or UK Biobank Axiom Array) with over 800,000 genome-wide markers⁵⁸. QC and imputation using the UK10K panel and the 1000 Genomes reference panels were performed centrally. For the present analysis, we excluded individuals with outliers for heterozygosity or genotype missingness, individuals with discordance between self-reported and genetically inferred sex, individuals with putative sex chromosome aneuploidy and individuals who decided to withdraw consent. In addition, we restricted ourselves to white British individuals as determined by previous principal component analysis⁵⁹ and kept only unrelated individuals (those with third degree or closer relationships were removed) while maximizing the final sample size⁶⁰. The final cohort consisted of 359,017 individuals (54% females; median

baseline age 59; median follow-up 7 years) of whom 15,208 had a high-quality 12-lead resting ECG. Genetic dosages of imputed variants (version 3) were used to calculate PRS_{BRS} using PLINK2 (ref.⁶¹). Scores were standardized so that the population mean was 0 and the s.d. was 1.

A PheWAS with an emphasis on cardiovascular traits was performed in this cohort using a list of 65 curated (disease) phenotypes (Supplementary Table 10). Associations between PRS_{BRS} and continuous phenotypes were tested using multivariable linear regression models in R v.3.5.0. Models were adjusted for age at baseline, sex, genotyping array and the first ten principal components of ancestry. Binary phenotypes were included if there were at least 500 cases and were assessed using multivariable logistic regression adjusted for the same covariates (Supplementary Table 11).

For associations between the PRS_{BRS} and ECG traits we further excluded: (1) individuals with heart rates over 120 b.p.m.; (2) individuals with previous myocardial infarction, Wolff–Parkinson–White syndrome or heart failure; (3) individuals with pacemakers; (4) individuals taking class 1 or class 3 antiarrhythmic or QT-prolonging medication (including digoxin); and (5) individuals with AF/flutter, atrioventricular block or any fascicular block on automated ECG. Trait-specific exclusions were also applied (Supplementary Table 12). Exclusions were based on previously published GWAS^{28–30} as well manual inspection of trait distributions. Associations were assessed using multivariable linear regression adjusted for age at ECG, sex, genotyping array, the first ten principal components of ancestry and optionally the RR-interval. Alpha for the entire PheWAS was determined at $0.05/70 = 7.00 \times 10^{-4}$ (Bonferroni correction).

Zebrafish model of MAPRE2 knockout. *Zebrafish maintenance.* Zebrafish (*Danio rerio*) were maintained in a dedicated fish facility at 28.5 °C with a stable circulating system that continuously filters, treats (with ultraviolet light) and aerates the water. All experiments using zebrafish followed animal protocols approved by the Harvard Medical School Institutional Animal Care and Use Committee and complied with ethical guidelines. For all zebrafish studies, wild-type embryos were injected at one-cell stage (as described under ‘Genome editing’) and used for experiments at 5 days postfertilization. Sex in zebrafish is not determined until adulthood around 2–3 months of age.

Genome editing. Wild-type (WT) AB/Tuebingen (AB/Tu) zebrafish were crossed and resultant embryos from the same clutches were divided into two different groups injected with a solution containing either three gRNAs targeting *mapre2* at three independent loci (exon 1: TGCTCGCCAGGGTCTGGAGGGGG, exon 3: TTCTTAAGACTGATACAGCCGGG, exon 4: GACAGAGCTTGGGT CGGACCGGG), Alt-R tracrRNA (catalog no. 1072533) and Alt-R S.p. HiFi Cas9 Nuclease V3 (catalog no. 1081060) or tracrRNA and Cas9 alone (all from Integrated DNA Technologies), according to the manufacturer’s instructions (Supplementary Fig. 7a). All larvae injected with gRNAs and used for optical mapping were sequenced using three primer pairs corresponding to the target sites of the three gRNAs: exon 1 (CTGTGAGTGGAGGacattc, CGCACTGTGTTCTTTCTGTAGG), exon 3 (TCATCTCTGTGCATTGTTTCC, CTGCACATGTCTAAAGCAAAGG) and exon 4 (CAACCTTGACTTCATTCAAGTG, acagaattccattcttgggtg). All larvae had evidence of editing at two loci or more by Sanger sequencing.

Optical mapping of isolated zebrafish hearts. Optical mapping and signal processing were performed as previously described⁶². Briefly, isolated hearts were incubated with a voltage-sensitive fluorescent dye in the FluoVolt Membrane Potential Kit (Invitrogen) for 20 min at room temperature. Subsequently, the hearts were transferred into a perfusion chamber (RC-49MFS; Warner Instruments) with Tyrode’s solution (room temperature) containing 136 mM NaCl, 5.4 mM KCl, 1.8 mM CaCl₂, 1.0 mM MgCl₂, 0.3 mM Na₂HPO₄, 5.0 mM glucose, 10 mM HEPES; pH 7.4 (NaOH). Cytochalasin D (1 mM; Sigma) was added to uncouple electrical impulses from contractions. The chamber was then mounted onto the stage of an inverted microscope (TW-2000; Nikon) with electrical wires connected to the built-in platinum wires in the chamber for pacing. The heart was excited with a 470-nm light-emitting diode, and the emission was collected by a high-speed 80 × 80 pixel CCD camera (RedShirtImaging) with 14-bit resolution. Using a ×20 objective and ×0.5 C-mount adapter, the final magnification was ×10 with a pixel-to-pixel distance of 2.4 μm. For signal processing and quantification, the images were analyzed by customized scripts in MATLAB (MathWorks)⁶². Optical mapping data are shown in Fig. 2a–c.

Quantitative real-time PCR on whole zebrafish larvae. Total RNA was extracted from whole 5-day postfertilization larvae using RNeasy Plus Mini Kit (Qiagen) and reversed transcribed using iScript Reverse Transcription Supremix for RT-qPCR (Bio-Rad), according to the manufacturers’ instructions. cDNA libraries were used for quantitative real-time PCR using iTaq Universal SYBR Green Supermix (Bio-Rad) on the CFX96 Touch Real-Time PCR Detection System (Bio-Rad). Samples were run in technical triplicates and data were analyzed using the delta–delta Ct method, normalized to the level of *eef1a* (Supplementary Fig. 7b,c and Supplementary Table 19).

Statistics. Data are presented as mean ± s.e.m. Data were analyzed using Excel. Groups were compared with unpaired two-tailed Student’s *t*-test and *P* < 0.05 defines statistical significance.

hiPSC-CM model of MAPRE2 knockout. *hiPSC maintenance.* The hiPSC line 19c3 was previously derived from peripheral blood mononuclear cells of a healthy male using Sendai virus (Invitrogen) and expressed an exogenous TNNT2 promoter-derived Zeocin resistance cassette⁶³. The hiPSCs were passaged at a ratio of ~1:15 every 4 days using 0.5 mM EDTA (for 6 min at room temperature), achieving ~75%–80% confluence. The cells were routinely maintained in B8 mediumX2 on 1:800 diluted growth factor reduced Matrigel (Corning), except for the first 24 h after passage when B8 was supplemented with 2 μM thiazovivin (LC Labs, T-9753), hereby referred to as B8T medium. All cultures (pluripotent and differentiation) were maintained in 2 ml of medium per 9.6 cm² of surface area or equivalent.

Genome editing. To generate MAPRE2 KO gRNA expression vectors, two gRNAs targeting all four splicing variants of MAPRE2 were designed using an online CRISPR design tool (IDT) with high predicted on-target score and minimal predicted off-target effect (Supplementary Fig. 8). DNA oligos (IDT) encoding each gRNA with BbsI ligation overhangs were annealed and inserted into the BbsI restriction site of a pSpCas9(BB)–2A–Puro (PX459, Addgene, catalog no. 62988) plasmid. The constructed gRNA expression plasmids were confirmed by Sanger sequencing (Eurofins) with the LK01_5_primer (5′-GACTATCATATGCTTACCG-3′). CRISPR–Cas9-mediated knockout of MAPRE2 was induced after cell passage by electroporation of 5×10^6 hiPSC with 5 μg of each gRNA expression vector. Subsequently, cells were maintained for 48 h in B8T medium supplemented with 0.5 μg ml^{−1} of puromycin (Gibco). Puromycin-resistant individual colonies were picked and expanded ~10 days after electroporation. Clones with indels were identified by genomic sequencing with primers outside the targeting region. Genomic DNA was extracted from the cell pellets using a Quick–DNA Miniprep Plus kit (Zymo).

hiPSC-CMs differentiation. Differentiation into hiPSC-CMs was performed according to previously described protocol with slight modifications^{64,65}. Briefly, at the start of differentiation (day 0), B8 medium was changed to R6C, consisting of RPMI 1640 (Corning, catalog no. 10-040-CM), supplemented with 6 μM of glycogen synthase kinase 3-β inhibitor CHIR99021 (LC Labs, catalog no. C-6556). On day 1, medium was changed to RPMI, and on day 2 medium was changed to RBA-C59, consisting of RPMI supplemented with 2 mg ml^{−1} fatty acid-free bovine serum albumin (GenDEPOT, A0100), 200 μg ml^{−1} L-ascorbic acid 2-phosphate (Wako, catalog no. 321-44823) and 0.5 μM Wnt-C59 (Biorbyt, catalog no. orb181132). Medium was then changed on day 4 and then every other day with RBAI media consisting of RPMI supplemented with 0.5 mg ml^{−1} fatty acid-free bovine serum albumin, 200 μg ml^{−1} L-ascorbic acid 2-phosphate and 1 μg ml^{−1} *Escherichia coli*-derived recombinant human insulin (Gibco, catalog no. A11382J). Contracting cells were noted from day 7, differentiated cardiomyocytes were treated with 25 μg ml^{−1} of Zeocin from day 10 to day 14. On day 20 of differentiation, cardiomyocytes were dissociated using DPBS for 20 min at 37 °C followed by 1:200 Liberase TH (Roche, catalog no. 5401151001) diluted in DPBS for 20 min at 37 °C, centrifuged at 300g for 5 min, and filtered through a 100 μm cell strainer (Falcon). hiPSC-CMs were then plated on a Matrigel-coated 18-mm cover glass (Warner Instruments) for action potential (AP) measurements and into 30-mm culture dishes for membrane current recordings.

Cellular electrophysiology of hiPSC-CMs. APs and membrane currents were measured with manual and automated patch-clamp, respectively. The experiments were not randomized and the investigators were blinded to allocation during experiments and outcome assessment. APs were recorded at 37 °C from spontaneously beating hiPSC-CMs using the amphotericin-B perforated patch-clamp technique with a Multiclamp 700B amplifier and Clampex v.10.3 software (Molecular Devices). Pipettes (resistance 3–3.5 MΩ) were pulled from thin wall borosilicate glass capillaries (WPI, catalog no. 1B120F-4) using a horizontal microelectrode puller (Sutter Instrument, catalog no. P-1000). Signals were low-pass-filtered with a cutoff of 10 kHz and digitized at 10 kHz. Bath solution contained: 140 mM NaCl, 4.0 mM KCl, 1.0 mM CaCl₂, 0.5 mM MgCl₂, 10 mM glucose, 10 mM HEPES; pH 7.4 (NaOH). Pipettes were filled with solution containing: 125 mM K-gluconate, 20 mM KCl, 5.0 mM NaCl, 0.26 mM amphotericin-B, 5.0 mM HEPES; pH 7.2 (KOH). To overcome the spontaneous activity and depolarized state of hiPSC-CMs⁶⁶, an ohmic current ~4 pA/pF was continuously injected to maintain a stable resting potential at approximately −80 mV, except where mentioned otherwise. The injected current did not differ significantly between the CTRL and MAPRE2 KO hiPSC-CMs (4.0 ± 0.2 pA (CTRL, *n* = 15) versus 4.3 ± 0.4 pA (MAPRE2 KO, *n* = 12)). APs were evoked at 1 Hz by 4-ms, ~1.3× threshold current pulses through the patch pipette, and were characterized by maximum AP amplitude, APD at 20% and 90% of repolarization (APD₂₀, APD₉₀, respectively) and *V*_{max}. The maximal diastolic potential was analyzed during spontaneous activity. Potentials were corrected for the calculated liquid junction potential⁶⁷.

I_{Na} and $I_{outward}$ were recorded at room temperature using a SyncroPatch 768 PE automated patch-clamp instrument (Nanion Technologies). Pulse generation and data collection were performed with PatchController384 v.1.3.0 and DataController384 v.1.2.1 (Nanion Technologies). Whole-cell currents were filtered at 3 kHz and acquired at 10 kHz. The access resistance and apparent membrane capacitance were estimated using built-in protocols. Series resistance was compensated for 95% and leak and capacitance artifacts were subtracted using the P/4 method. Seal resistance was 0.54 ± 0.05 G Ω (average \pm s.e.m., $n = 234$), and cells were excluded from analysis if the maximum peak I_{Na} amplitude was less than 300 pA.

For the automated patch-clamp recordings, hiPSC-CMs were plated into 30-mm culture dishes 5 days before the experiment. The day of the experiment, cells were washed once with DPBS^{-/-} for 20 min. Cells were then detached with 5 min treatment of TrypLE followed by 20–30 min treatment with RBAI media with 1:200 dilution of Liberase TH. Cells were then re-suspended in 15% RBAI media and 85% external solution at 180,000 cells ml⁻¹. Cells were allowed to recover for at least 30 min at 15°C while shaking on a rotating platform. Following equilibration, 10 μ l of cell suspension was added to each well of a 384-well, single-hole, low resistance (2 M Ω) for I_{Na} study and medium resistance (4 M Ω) for $I_{outward}$ study 'chip' (Nanion Technologies). The external solution contained: 140 mM NaCl, 4.0 mM KCl, 2.0 CaCl₂, 1.0 mM MgCl₂, 5.0 mM glucose 5, 10 mM HEPES; pH 7.4 (NaOH). The internal solution to study I_{Na} contained: 110 mM CsF, 10 mM CsCl, 10 mM NaCl, 10 mM EGTA, 10 mM HEPES; pH 7.2 (CsOH). The internal solution to study $I_{outward}$ contained: 60 mM KF, 50 mM KCl, 10 mM NaCl, 10 EGTA, 10 mM HEPES; pH 7.2 (KOH).

I_{Na} was measured using a double-pulse protocol (Fig. 2f, inset left panel) from a holding potential of -120 mV (cycle length of 5 s). I_{Na} was defined as the difference between peak and steady-state current and current densities were calculated by dividing current amplitude by C_m . Recovery from inactivation was measured using a two-pulse protocol, where a conditioning pulse -20 mV inactivated Na⁺ channels, followed by a test pulse to -20 mV after a variable recovery interval ranging between 1 and 5,000 ms at -120 mV. Voltage dependence of activation and inactivation curves were fitted with Boltzmann function ($y = [1 + \exp\{(V - V_{1/2})/k\}]^{-1}$), where $V_{1/2}$ is the half-maximal voltage of (in)activation and k , the slope factor. $I_{outward}$ was acquired with a double-pulse protocol (Fig. 2f, inset right panel) from a holding potential of -80 mV (cycle length of 10 s). $I_{outward}$ was measured at the end of the first pulse and densities were calculated by dividing current amplitude by C_m .

Quantitative real-time PCR. RNA was isolated using TRI reagent (Zymo) and Direct-zol RNA microprep kit (Zymo) including on-column DNase digestion to remove genomic DNA. cDNA was produced from 2 μ g of total RNA using a High Capacity RNA-to-cDNA kit (Applied Biosystems). All PCR reactions were performed in triplicate in a 384-well plate format using TaqMan Gene Expression Master Mix in a QuantStudio 5 Real-Time PCR System (both Applied Biosystems) with following TaqMan Gene Expression Assays (Applied Biosystems): 18S (Hs99999901_s1), ACTB (Hs01060665_g1), GAPDH (Hs02786624_g1) and MAPRE2 (Hs00936741_m1). Relative quantification of gene expression was calculated using 2^{- $\Delta\Delta$ Ct} method, normalized to the reference 18S, ACTB or GAPDH and untreated control samples as specified in Supplementary Fig. 7.

Statistics. Data were presented as mean \pm s.e.m.. Data were analyzed and graphed in GraphPad Prism 8. Comparisons were conducted via two-way analysis of variance and unpaired two-tailed Student's t -test. A P value < 0.05 defines statistical significance. The experiments were not randomized and the investigators were blinded to allocation during experiments and outcome assessment.

Reporting Summary. Further information on research design is available in the Nature Research Reporting Summary linked to this article.

Data availability

Data from the Genome Aggregation Database (gnomAD, v2.1) are available at <https://gnomad.broadinstitute.org>. Data from the UK Biobank participants can be requested from the UK Biobank Access Management System (<https://bbams.ndph.ox.ac.uk>). Data from the Genotype Tissue Expression (GTEx) consortium are available at the GTEx portal (<https://gtexportal.org>) accessed December 2019 and March 2020. The Molecular Signatures Database (MSigDB, v6.2) is available at <http://www.gsea-msigdb.org/gsea/index.jsp>. Other datasets generated during and/or analyzed during the current study can be made available upon reasonable request to the corresponding authors. Individual-level data sharing is subject to restrictions imposed by patient consent and local ethics review boards. The Brugada syndrome GWAS summary statistics are available on Zenodo, at <https://doi.org/10.5281/zenodo.5095177> and on the GWAS catalog database (study ID accession: GCST90086158). The BrS polygenic score is available on the PGS catalog (PGS ID accession: PGS001779).

References

34. Priori, S. G. et al. Executive summary: HRS/EHRA/APHR expert consensus statement on the diagnosis and management of patients with inherited primary arrhythmia syndromes. *Europace* **15**, 1389–1406 (2013).

35. Al-Khatib, S. M. et al. 2017 AHA/ACC/HRS guideline for management of patients with ventricular arrhythmias and the prevention of sudden cardiac death: executive summary: a report of the American College of Cardiology/American Heart Association Task Force on Clinical Practice Guidelines and the Heart Rhythm Society. *Circulation* **138**, e210–e271 (2018).
36. Richards, S. et al. Standards and guidelines for the interpretation of sequence variants: a joint consensus recommendation of the American College of Medical Genetics and Genomics and the Association for Molecular Pathology. *Genet. Med.* **17**, 405–423 (2015).
37. Whiffin, N. et al. CardioClassifier: disease- and gene-specific computational decision support for clinical genome interpretation. *Genet. Med.* **20**, 1246–1254 (2018).
38. Kapplinger, J. D. et al. An international compendium of mutations in the SCN5A-encoded cardiac sodium channel in patients referred for Brugada syndrome genetic testing. *Heart Rhythm* **7**, 33–46 (2010).
39. Walsh, R., Peters, N. S., Cook, S. A. & Ware, J. S. Paralogous annotation identifies novel pathogenic variants in patients with Brugada syndrome and catecholaminergic polymorphic ventricular tachycardia. *J. Med. Genet.* **51**, 35–44 (2014).
40. Denham, N. C. et al. Systematic re-evaluation of SCN5A variants associated with Brugada syndrome. *J. Cardiovasc. Electrophysiol.* **30**, 118–127 (2019).
41. Walsh, R. et al. Quantitative approaches to variant classification increase the yield and precision of genetic testing in Mendelian diseases: the case of HCM. *Genome Med.* **11**, 5 (2019).
42. Das, S. et al. Next-generation genotype imputation service and methods. *Nat. Genet.* **48**, 1284–1287 (2016).
43. Yang, J. et al. Common SNPs explain a large proportion of the heritability for human height. *Nat. Genet.* **42**, 565–569 (2010).
44. Yang, J., Lee, S. H., Goddard, M. E. & Visscher, P. M. GCTA: a tool for genome-wide complex trait analysis. *Am. J. Hum. Genet.* **88**, 76–82 (2011).
45. Lee, S. H., Wray, N. R., Goddard, M. E. & Visscher, P. M. Estimating missing heritability for disease from genome-wide association studies. *Am. J. Hum. Genet.* **88**, 294–305 (2011).
46. Vutthikraivit, W. et al. Worldwide prevalence of Brugada syndrome: a systematic review and meta-analysis. *Acta Cardiol. Sin.* **34**, 267–277 (2018).
47. Machiela, M. J. & Chanock, S. J. LDlink: a web-based application for exploring population-specific haplotype structure and linking correlated alleles of possible functional variants. *Bioinformatics* **31**, 3555–3557 (2015).
48. Hormozdizari, F. et al. Colocalization of GWAS and eQTL signals detects target genes. *Am. J. Hum. Genet.* **99**, 1245–1260 (2016).
49. Watanabe, K., Taskesen, E., van Bochoven, A. & Posthuma, D. Functional mapping and annotation of genetic associations with FUMA. *Nat. Commun.* **8**, 1826 (2017).
50. Schmitt, A. D. et al. A compendium of chromatin contact maps reveals spatially active regions in the human genome. *Cell Rep.* **17**, 2042–2059 (2016).
51. Pers, T. H., Timshel, P. & Hirschhorn, J. N. SNPsnap: a Web-based tool for identification and annotation of matched SNPs. *Bioinformatics* **31**, 418–420 (2015).
52. Leeuw, C. A., de, Mooij, J. M., Heskes, T. & Posthuma, D. MAGMA: generalized gene-set analysis of GWAS data. *PLoS Comput. Biol.* **11**, e1004219 (2015).
53. Subramanian, A. et al. Gene set enrichment analysis: a knowledge-based approach for interpreting genome-wide expression profiles. *Proc. Natl Acad. Sci. USA* **102**, 15545–15550 (2005).
54. Finucane, H. K. et al. Partitioning heritability by functional annotation using genome-wide association summary statistics. *Nat. Genet.* **47**, 1228–1235 (2015).
55. Backenroth, D. et al. FUN-LDA: a latent dirichlet allocation model for predicting tissue-specific functional effects of noncoding variation: methods and applications. *Am. J. Hum. Genet.* **102**, 920–942 (2018).
56. Willer, C. J., Li, Y. & Abecasis, G. R. METAL: fast and efficient meta-analysis of genomewide association scans. *Bioinformatics* **26**, 2190–2191 (2010).
57. Sudlow, C. et al. UK Biobank: an open access resource for identifying the causes of a wide range of complex diseases of middle and old age. *PLoS Med.* **12**, e1001779 (2015).
58. Bycroft, C. et al. The UK Biobank resource with deep phenotyping and genomic data. *Nature* **562**, 203–209 (2018).
59. Aragam, K. G. et al. Phenotypic refinement of heart failure in a national biobank facilitates genetic discovery. *Circulation* <http://dx.doi.org/CIRCULATIONAHA.118.035774> (2018).
60. Choi, S. H. et al. Monogenic and polygenic contributions to atrial fibrillation risk: results from a national biobank. *Circ. Res.* **126**, 200–209 (2020).
61. Chang, C. C. et al. Second-generation PLINK: rising to the challenge of larger and richer datasets. *Gigascience* **4**, 7 (2015).
62. Panáková, D., Werdich, A. A. & Macrae, C. A. Wnt11 patterns a myocardial electrical gradient through regulation of the L-type Ca(2+) channel. *Nature* **466**, 874–878 (2010).
63. Kuo, H.-H. et al. Negligible-cost and weekend-free chemically defined human iPSC culture. *Stem Cell Rep.* **14**, 256–270 (2020).

64. BurrIDGE, P. W., Holmström, A. & Wu, J. C. Chemically defined culture and cardiomyocyte differentiation of human pluripotent stem cells. *Curr. Protoc. Hum. Genet.* **87**, 21.3.1–21.3.15 (2015).
65. BurrIDGE, P. W. et al. Chemically defined generation of human cardiomyocytes. *Nat. Methods* **11**, 855–860 (2014).
66. Veerman, C. C. et al. Immaturity of human stem-cell-derived cardiomyocytes in culture: fatal flaw or soluble problem? *Stem Cells Dev.* **24**, 1035–1052 (2015).
67. Barry, P. H. & Lynch, J. W. Liquid junction potentials and small cell effects in patch-clamp analysis. *J. Membr. Biol.* **121**, 101–117 (1991).
68. Bravo, E. et al. Developing a guideline to standardize the citation of bioresources in journal articles (CoBRA). *BMC Med.* **13**, 33 (2015).
69. Wang, Y. et al. The 3D Genome Browser: a web-based browser for visualizing 3D genome organization and long-range chromatin interactions. *Genome Biol.* **19**, 151 (2018).

Acknowledgements

We are greatly indebted to the patients included in the study. We thank V. Cotard, C. Goutsméd, M.-F. Le Cunff and N. Bourgeois for assistance in patient recruitment and L. Beekman for his technical support. We thank the biological resource centre for biobanking (CHU Nantes, Nantes Université, Centre de ressources biologiques (BB-0033-00040), F-44000 Nantes, France) for applying the following guidelines⁴⁸. We are most grateful to the Genomics and Bioinformatics Core Facility of Nantes (GenoBiRD, Biogenouest, IFB) for its technical support. This research has been conducted using the UK Biobank resource; we are grateful to UK Biobank participants. The MINE study (J.H.V.) has received funding from the European Research Council (ERC) under the European Union's Horizon 2020 research and innovation program (grant agreement no. 772376—ESCORIAL). The collaboration project is cofunded by the PPP Allowance made available by Health—Holland, Top Sector Life Sciences & Health, to stimulate public–private partnerships. This study makes use of data generated by the Wellcome Trust Case-Control Consortium. A full list of the investigators who contributed to the generation of the data is available from www.wtccc.org.uk. Funding for the project was provided by the Wellcome Trust under award 076113, 085475 and 090355. The KORA research platform (KORA, Cooperative Research in the Region of Augsburg) was initiated and financed by the Helmholtz Zentrum München—German Research Center for Environmental Health, which is funded by the German Federal Ministry of Education and Research and by the State of Bavaria. Furthermore, KORA research was supported within the Munich Center of Health Sciences (MC Health), Ludwig-Maximilians-Universität, as part of LMUinnovativ. J. Barc is supported by the research program Etoiles montantes des Pays de la Loire REGIOCARD RPH081-U1087-REG-PDL, ANR JCJC LEARN (R21006NN, RPV21014NNA) and by the H2020-MSCA-IF-2014 Program of the European Commission (RISTRAD-661617). R.T. is supported by the Canadian Heart Rhythm Society's George Mines Award, the European Society of Cardiology research award, and the Philippa and Marvin Carsley Cardiology Chair. D.Y.C. is supported by Fondation Leducq and National Institutes of Health (NIH) NHGRI T32 (no. 1T32HG010464-01). M. Baudic was supported by IRP—VERACITIES—New Mechanisms for VEntricular ARrhythmia And CardIomeTabolic DiseaseS, an I-SITE NExT health and engineering initiative (Ecole Centrale and Nantes University) and by the IRP—GAINES—Genetic Architecture IN cardiovascular disEaSeS funded by INSERM and CNRS. R.W. is supported by an Amsterdam Cardiovascular Sciences fellowship. S.C. is supported by the NHLBI BioData Catalyst Fellows Program. C.A.R. is supported by Fondation Leducq, the Dutch Heart Foundation (CVON PREDICT2) and the Innovational Research Incentives Scheme Vidi grant from the Netherlands Organisation for Health Research and Development (ZonMw; 91714371). Y.D.W. is supported by the Robert Lancaster Memorial Fund. M.P. is supported by Cardiac Risk in the Young. S.V.D. is supported by Wetenschappelijk Fonds Willy Gepts VUB-UZ Brussel, project 'Unravelling the molecular genetic pathways of Brugada Syndrome by cardiomics research', VUB IRP project 'IMAGica: an Integrative personalized Medical Approach for Genetic diseases, Inherited Cardia Arrhythmias as a model' and Innoviris BRIDGE 2017, project 'IGenCare: Integrated Personalised Medical Genomics Care Solution for Patients with Rare Genetic Diseases'. S.H. is supported by the Barts BRC. B.R. is supported by the DZHK (German Centre

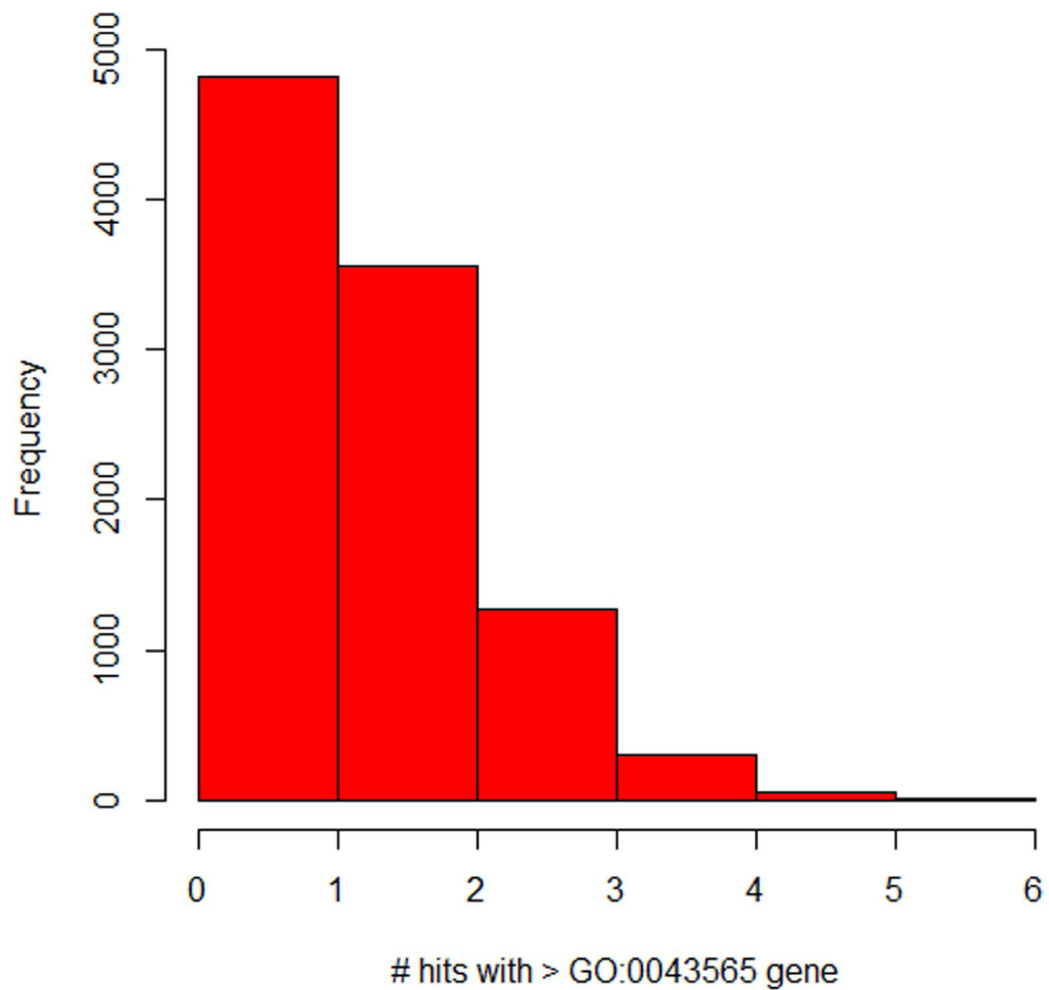
for Cardiovascular Research) and by the BMBF (German Ministry of Education and Research). B.G.W. is supported by the Danish Heart Foundation. M.B.S. is supported by K23HL127704. Project MinE Belgium was supported by a grant from IWT (no. 140935), the ALS Liga België, the National Lottery of Belgium and the KU Leuven Opening the Future Fund. D.C. and C.L. are supported by HYPERGENES (HEALTH-F4-2007). D.R. is supported by R01 HL149826, P50 GM115305. P.J.S. acknowledges the support of Leducq Foundation for Cardiovascular Research grant 18CVD05. P.V.D. is supported by the Netherlands CardioVascular Research Initiative (CVON PREDICT2). C.A. is supported by NIH HL47678 and HL138103, W.W. Smith Charitable Trust and Wistar Morris Fund. M.B. is Supported by the DZHK (German Centre for Cardiovascular Research) and by the BMBF (German Ministry of Education and Research). P.D.L. is supported by UCL/UCLH Biomedicine NIHR and Barts BRC. B.L. is supported by GOA—Antigone 33933. J.B. is supported by a Senior Clinical Fellowship of the Flemish Science Foundation (FWO). E.B. is supported by the British Heart Foundation including BHF Clinical Research Training Fellowship (FS/11/71/28918: Future diagnostic role and new genetic loci in SADS), Cardiac Risk in the Young and Robert Lancaster Memorial fund sponsored by McColl's Ltd. Retail Group. H.L.T. is supported by the European Union's Horizon 2020 research and innovation program under acronym ESCAPE-NET, registered under grant agreement no. 733381, and the Dutch Heart Foundation (CVON RESCUE and PREDICT2 projects). M.D. is supported by NIH-RO1 HL134328. P.T.E. was supported by the Fondation Leducq (14CVD01), the NIH (1R01HL092577, R01HL128914, K24HL105780), the American Heart Association (18SFRN34110082) and by a research grant from Bayer AG to the Broad Institute. S.A.L. is supported by NIH grant 1R01HL139731 and American Heart Association 18SFRN34250007. J.-B.G. received a grant from the Fédération Française de Cardiologie (PREVENT project). A.L.G. is supported by the Fondation Leducq. C.A.M.R. is supported by the Leducq Foundation and Burroughs Wellcome Fund. A.A.W. is supported by the Dutch Heart Foundation (CVON PREDICT2 project). J.-J.S. is supported by the Fondation pour la Recherche Médicale (DEQ20140329545). R.R. and P.G. are supported by the National Agency for Research (ANR-GENSUD-14-CE10-0001). C.R.B. is supported by the Dutch Heart Foundation (CVON PREDICT2 project), the Netherlands Organization for Scientific Research (VICI fellowship, 016.150.610) and Fondation Leducq (17CVD02).

Author contributions

J. Barc, R.T., C. Glinge, D.Y.C., M.J., J.-J.S., P.W.B., A.L.G., C.A.M.R., C.D., M.W.T., R.R. and C.R.B. conceived/designed elements of the study. All authors acquired, analyzed or interpreted data. J. Barc, R.T., C. Glinge, D.Y.C., M.J., A.O.V., J.-J.S., P.W.B., A.L.G., C.A.M.R., C.D., M.W.T., A.A.W., R.R. and C.R.B. drafted the manuscript. All authors critically revised the manuscript for important intellectual content and approved the final version.

Competing interests

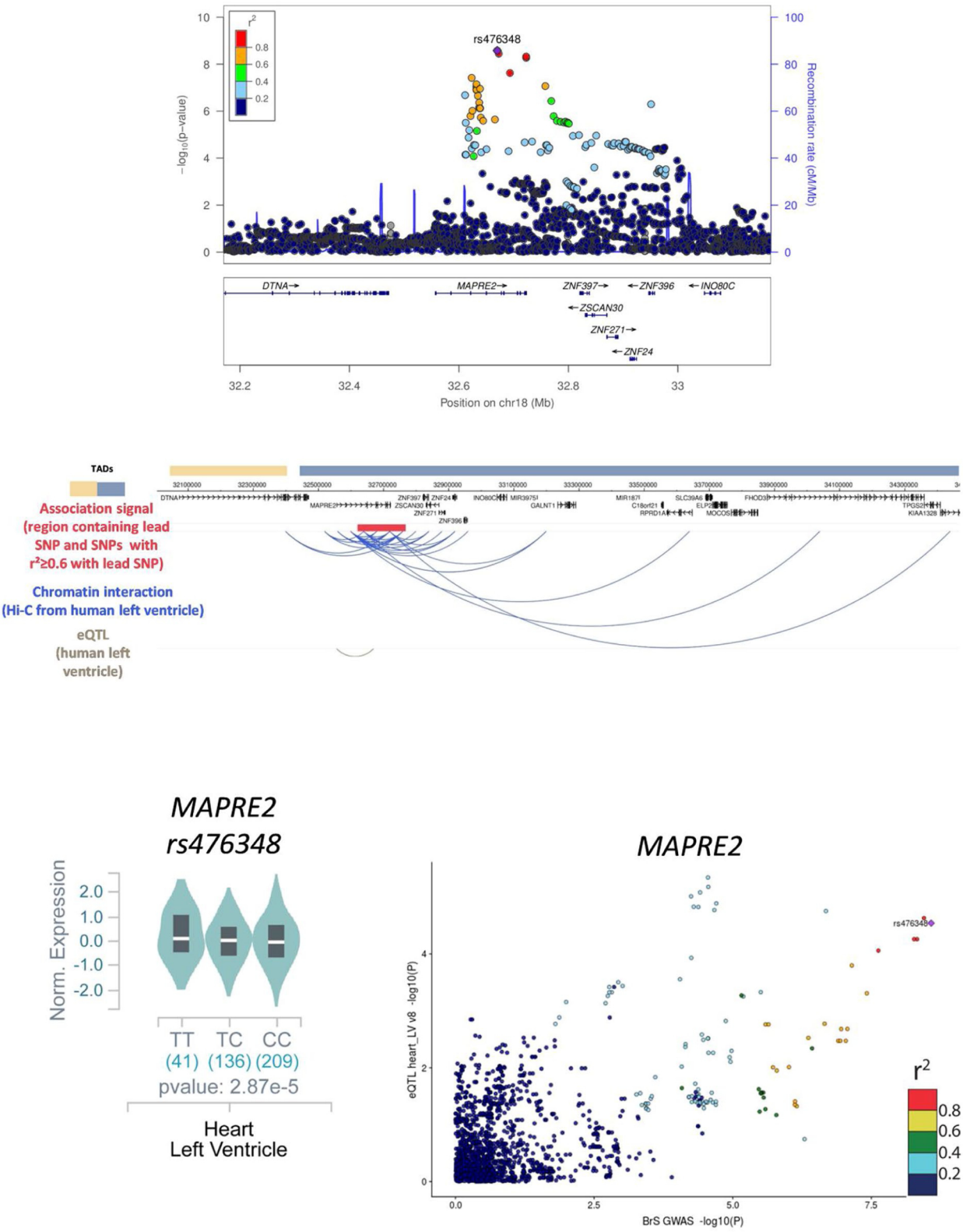
P.V.D. holds a senior clinical investigatorship of FWO-Vlaanderen and is supported by the E. von Behring Chair for Neuromuscular and Neurodegenerative Disorders. S.A.L. receives sponsored research support from Bristol Myers Squibb/Pfizer, Bayer AG, Boehringer Ingelheim and Fitbit, and has consulted for Bristol Myers Squibb/Pfizer and Bayer AG, and participates in a research collaboration with IBM. P.T.E. has served on advisory boards or consulted for Bayer AG, Quest Diagnostics, MyoKardia and Novartis. A.L.G. is part of the Scientific Advisory Board for Amgen, Inc. The remaining authors declare no competing interests.



Extended Data Fig. 1 | Developmental transcription factor gene enrichment. In 10,000 simulations of 12 SNP sets matching the non-chromosome 3 BrS lead SNPs (permutation-based unilateral (one-sided P -value) enrichment test), no more than six DNA binding protein genes were located within 300 kb (range: 0-6 genes). In contrast, among the 12 non-chromosome 3 lead SNPs, 10 overlapped or were located within 300 kb of DNA binding protein genes ($P=1 \times 10^{-4}$). DNA binding protein genes were defined according to number of Gene Ontology: 0043565.

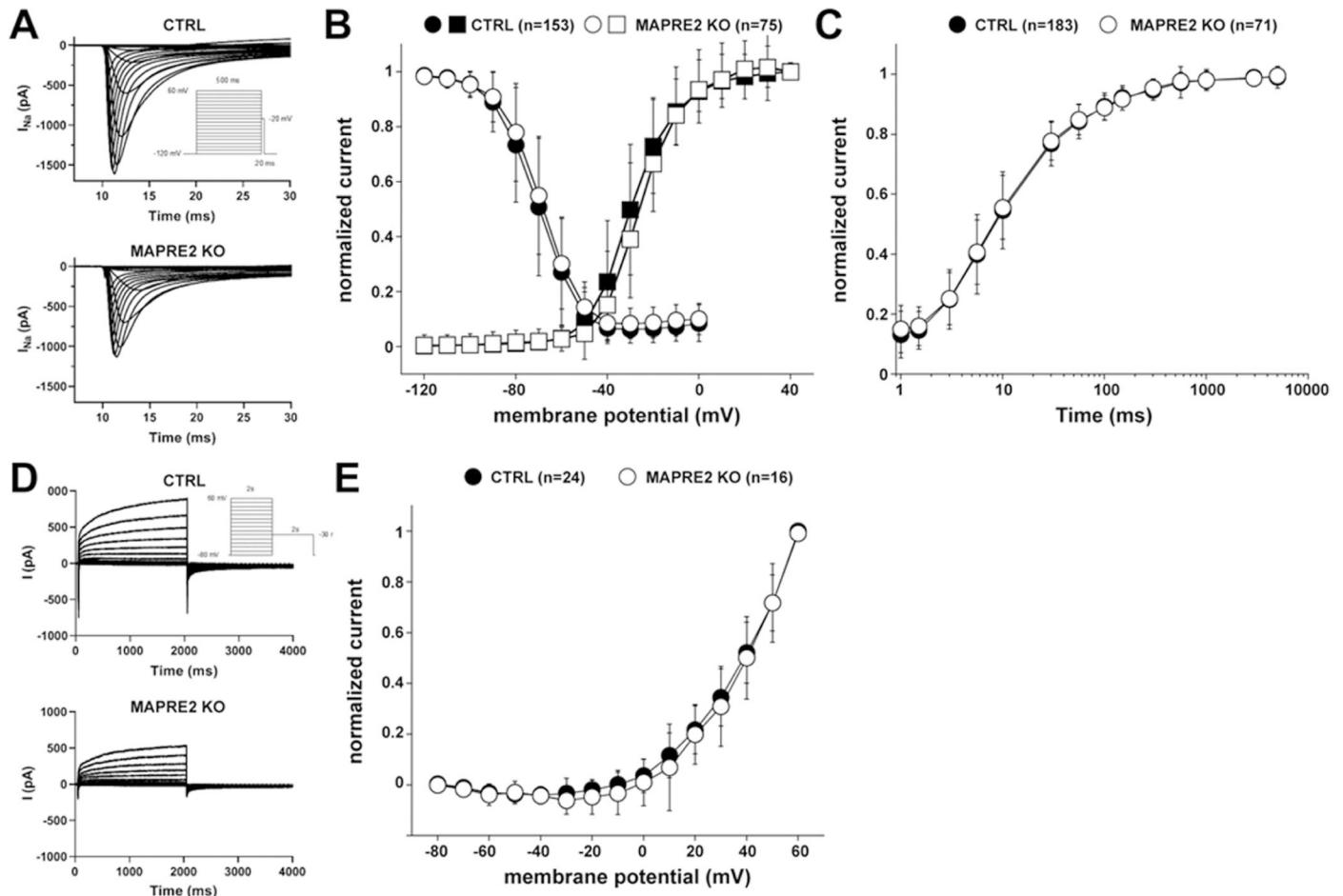
rs476348 18:32670021

rs476348

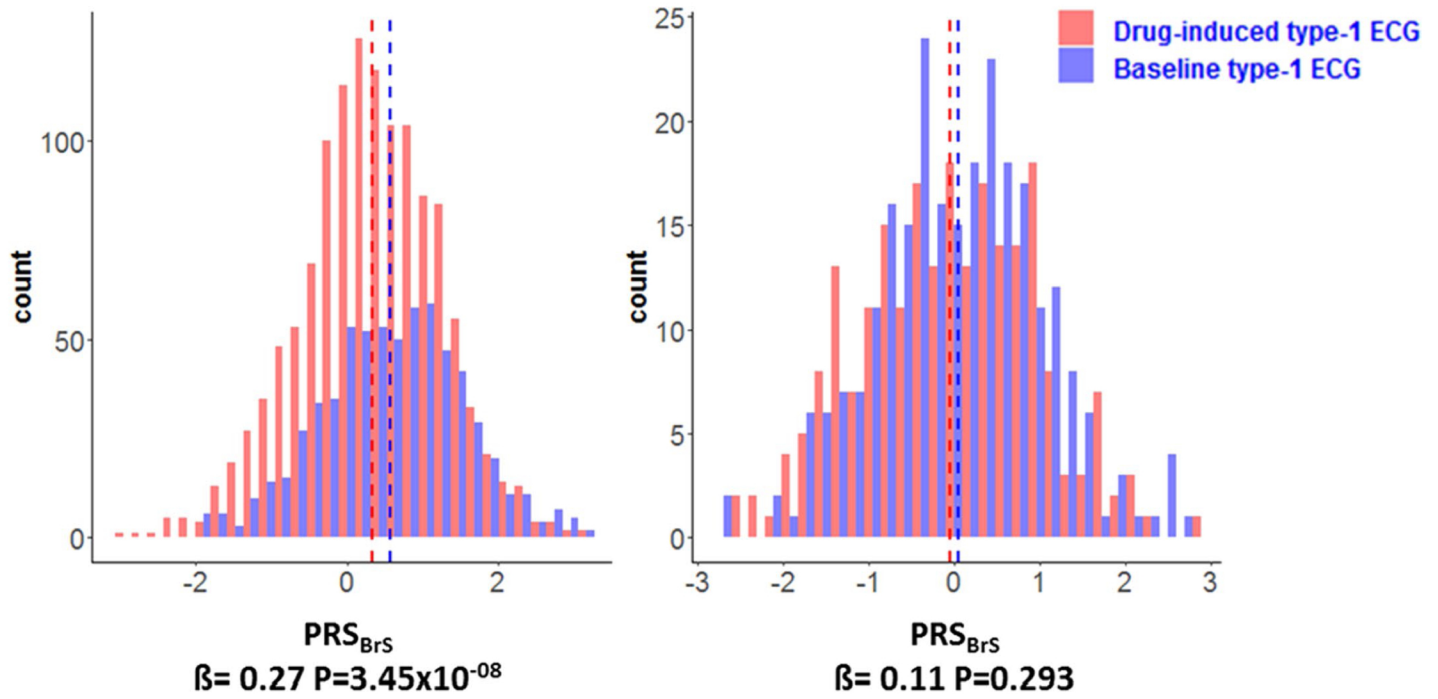


Extended Data Fig. 2 | See next page for caption.

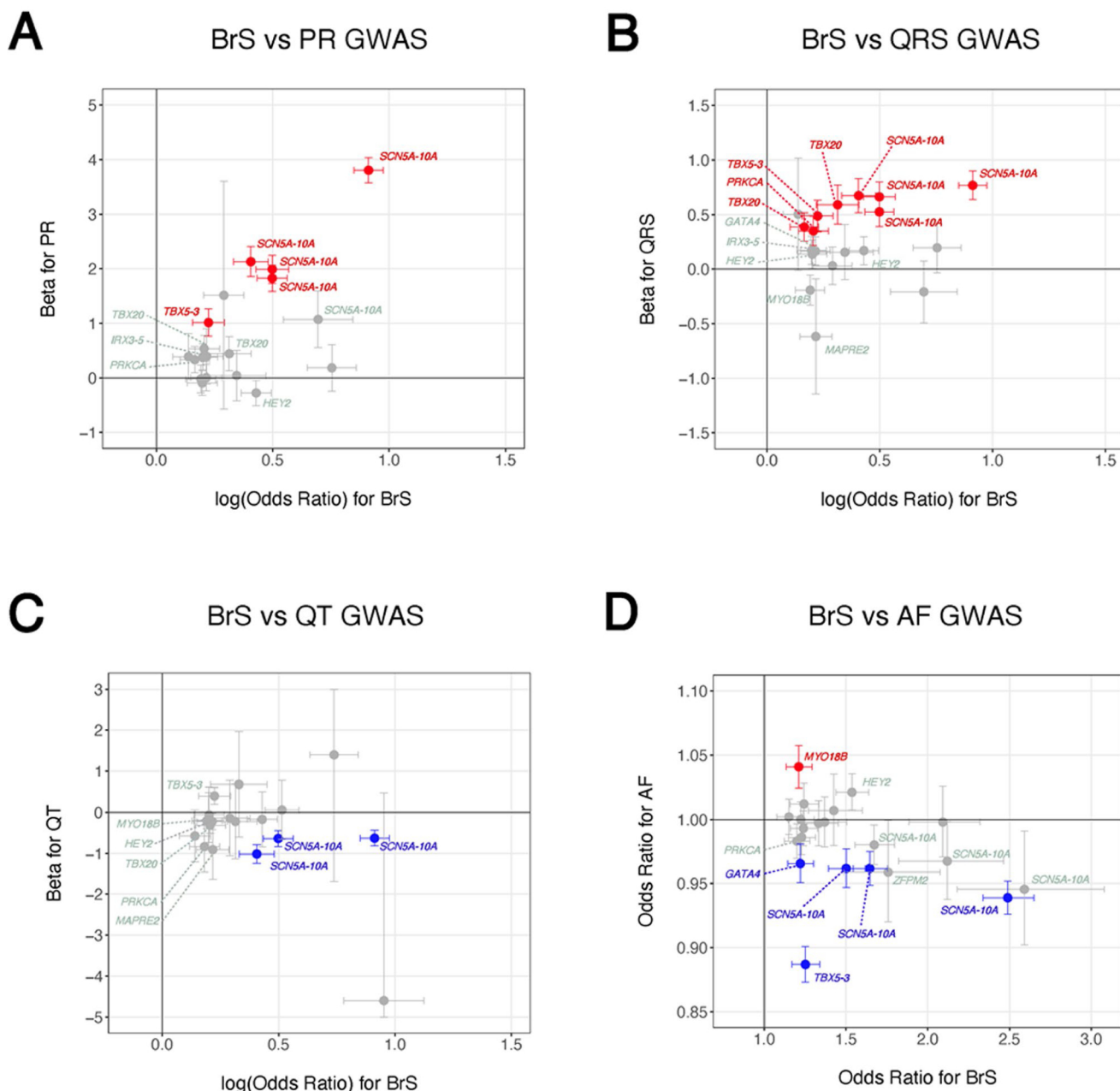
Extended Data Fig. 2 | Annotation of the chromosome 18 locus. Top panel, Locus Zoom plot of BrS associated variant at the chromosome 18 locus based on the meta-analysis data. $-\log_{10} P$ -values are shown along the left y-axis, and the right y-axis corresponds to recombination rate, plotted as a blue line. The x-axis indicates chromosomal position. The lead variant at each association signal is shown as a purple diamond. Other variants are colored according to their correlation (r^2) with the lead variant (see legend). Middle panel, Graphic representation of the chromosome 18 locus displaying the following annotations: genomic coordinates (hg19), topologically associated domains (TAD)⁶⁹; region containing SNPs in linkage disequilibrium with the lead SNP at the locus (red bar, LD, $r^2 \geq 0.6$); genes located in the locus; chromatin interactions identified in human left ventricular tissue⁵¹ overlapping the association signal (± 40 kb corresponding to the Hi-C dataset resolution), and expression quantitative trait loci (eQTL) reported in GTEx²⁰ for human left ventricular tissue. Bottom left panel, eQTL violin plot from GTEx displaying significant association between the lead SNP of the chromosome 18 locus and the expression of *MAPRE2* within the cardiac ventricular tissue. The number of left ventricular heart samples per genotype is shown in parentheses. In the box plots, the middle line shows the median value of the expression of each genotype, while the violin plots show the distribution. Bottom right panel, Locus compare plot depicting SNPs at the chromosome 18 locus. The eQTL $-\log_{10} P$ -value is plotted on the y-axis, and the BrS GWAS meta-analysis $-\log_{10} P$ -value is plotted on the x-axis. SNPs are colored according to their degree of linkage disequilibrium (r^2), with the lead BrS associated variant highlighted as a purple diamond. eQTL, expression quantitative trait locus. Note that a different scale is used in the top and middle panels.



Extended Data Fig. 3 | Cellular electrophysiology studies in MAPRE2 knockout and control hiPSC-CMs. Typical current recordings and (in)activation properties in control (CTRL) human induced pluripotent stem cell derived cardiomyocytes (hiPSC-CMs) and without MAPRE2 (MAPRE2 KO). **a**, Typical sodium current (I_{Na}) in a CTRL and MAPRE2-KO hiPSC-CM. **b**, Voltage-dependency of activation (squares) and inactivation (circles) in CTRL and MAPRE2 KO hiPSC-CMs. The $V_{1/2}$ of voltage dependency of activation was 4.2 mV more positive ($P=0.0016$) in MAPRE2 KO compared with CTRL hiPSC-CMs. **c**, Recovery from inactivation in CTRL and MAPRE2 KO hiPSC-CMs. **d**, Typical repolarizing outward currents ($I_{Outward}$) in a CTRL and a MAPRE2 KO hiPSC-CM. **e**, Voltage-dependency of $I_{Outward}$ activation in CTRL and MAPRE2 KO hiPSC-CMs. CTRL, control; KO, knock-out. Data in **b**, **c**, and **e** are presented as mean values \pm s.e.m. Statistical test used was two-sided unpaired t -test.



Extended Data Fig. 4 | Distribution of PRS_{BrS} in specific patient sub-groups. Histograms displaying distribution of PRS_{BrS} in specific patient sub-groups. **a**, PRS_{BrS} distribution comparing $SCN5A^-$ BrS cases presenting with a spontaneous type 1 BrS ECG with $SCN5A^-$ BrS cases presenting with a type 1 BrS ECG after sodium channel blocker challenge (drug-induced). **b**, PRS_{BrS} distribution comparing $SCN5A^+$ BrS cases presenting with a type 1 ECG at baseline with $SCN5A^+$ BrS cases presenting with a type 1 BrS ECG after sodium channel blocker challenge. PRS_{BrS} was calculated per individual based on the 21 BrS risk alleles and their corresponding effect sizes. Results were obtained after logistic regression, two-sided P -value not corrected for multiple testing. Reported P -values refer to the difference in PRS_{BrS} units between two groups.



Extended Data Fig. 5 | Comparison of effect on BrS susceptibility with effect on ECG intervals (PR, QRS and QT) and AF susceptibility from previously published GWAS. a-d, Effect size of the BrS risk alleles compared to their respective effect size on PR-interval (**a**), QRS-duration (**b**), QT-interval (**c**) and AF risk (**d**). In all panels, the x-axis represents the effect on BrS susceptibility from the BrS GWAS meta-analysis, presented either as log(odds ratios) with 95% confidence intervals (**a-c**), or as odds ratios with 95% confidence intervals (**d**). For **a-c**, the y-axis represents the effect estimates and 95% confidence interval (milliseconds per allele) calculated for PR-interval, QRS-duration or QT-interval in previously published GWAS conducted in the general population⁴⁻⁶. For **d**, the y-axis represents the effect on AF susceptibility from previously published GWAS⁷, shown as odds ratios with 95% confidence intervals. Red color indicates that the BrS risk allele (or a proxy with $r^2 > 0.8$) is associated with a prolongation of the ECG parameter or an increased risk of AF in the published GWAS at $P < 1 \times 10^{-5}$, while blue color indicates that the BrS risk allele is associated with a shorter ECG interval or a decreased risk of AF at $P < 1 \times 10^{-5}$. Loci annotated with a gene name in grey reached at least nominal significance in the published GWAS ($P < 0.05$). BrS, Brugada syndrome; AF, atrial fibrillation or flutter; PR, PR-interval; QRS, QRS-duration; QT, QT-interval; OR, odds ratio. Effect sizes of all 21 BrS susceptibility SNPs or their proxies on PR-interval, QRS-duration, QT-interval and AF risk in previous GWAS studies are listed in Supplementary Tables 14-17.